Communications Research Centre

A SAW-BASED DEMODULATOR FOR MULTIPLE-USER DEHOPPED M-ARY FSK SIGNALS IMPLEMENTATION AND MEASUREMENTS

by

E.B. Felstead, J.L. Pearce, and D.L. Selin

This document was prepared for and is the property of the Department of National Defence, Research and Development Branch under Project No. 32A58.

Government of Canada
Department of Communications

Gouvernement du Canada
Ministère des Communications

CRC REPORT NO. 1392
OTTAWA, JUNE 1985

Canada

COMMUNICATIONS RESEARCH CENTRE

DEPARTMENT OF COMMUNICATIONS
CANADA

A SAW-BASED DEMODULATOR FOR MULTIPLE-USER DEHOPPED M-ARY FSK SIGNALS -- IMPLEMENTATION AND MEASUREMENTS

by

E.B. Felstead, J.L. Pearce, and D.L. Selin

(Space Technology and Applications Branch)

CRC REPORT NO. 1392

June 1985
OTTAWA

This document was prepared for and is the property of the Department of National Defence, Research and Development Branch under Project No. 32A58.

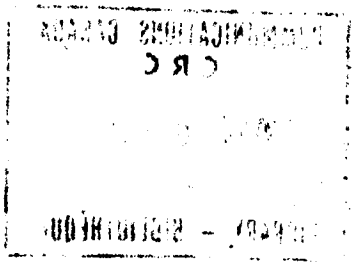

CONTENTS

A SAW-BASED DEMODULATOR FOR MULTIPLE-USER DEHOPPED M-ARY FSK SIGNALS-IMPLEMENTATION AND MEASUREMENTS

by

E.B. Felstead, J.L. Pearce, and D.L. Selin

ABSTRACT

A demodulator has been built and tested that is capable of performing the functions of an onboard-the-satellite processor for receiving M-ary noncoherent FSK signals with multiple users being separated by FDMA. It is based on spectral analysis of the received signal by a chirp transformer implemented with surface acoustic-wave devices. Demodulation of M=4-, 8-, and 16-ary FSK signals of 25 μs symbol duration was demonstrated with capability of handling up to 40/M users. The implementation loss was only 0.5 dB. Measurement of bit error rate performance in the presence of system noise, frequency errors, and partial-band-noise and multiple-tone jamming were made and found to agree well with theory. The effects were examined of three different time windows: rectangular, Kaiser Bessel $\alpha = 1.6$, and one intermediate between these two. The intermediate window is promising because of low window loss combined with good adjacent channel interference tolerance.

1. INTRODUCTION

For a number of EHF military satellite communications systems under current consideration, the uplink will use M-ary noncoherent FSK (NCFSK) modulation with multiple users being separated by frequency-division multiple access (FDMA). These systems are for low data-rate signals ($\leq$2.4 kb/s). Fast frequency hopping is used for uplink anti-jam protection.

For these systems it is required to dehop the uplink signal onboard the satellite and then to demodulate the dehopped signals. In this report, a laboratory implementation of such a demodulator is described. It was incorporated into a powerful measurement system that could generate and demodulate M=4-, 8-, and 16-ary NCFSK signals and handle up to 40/M users simultaneously. The performance in the presence of system noise, frequency errors, and various forms of jamming, including partial-band noise and multiple-tone, were measured and are given here. By switching the jamming on and off appropriately, the effect of partial band jamming was achieved without the necessity of hopping and dehopping. Because of a variable

window function capability, new insights were gained on window effects related to jammers and interchannel interference.

The required receiver for M-ary noncoherent FSK (NCFSK) signals uses matched filter energy detection. The matched filtering can be implemented in a number of ways. The direct way is to use a bank of M matched filters, one for each of the M possible frequency tones. An indirect implementation is to use a Fourier transform followed by sampling at the tone spacing; it is mathematically equivalent to the matched filter method. For multiple users separated via FDMA, a Fourier transformer becomes an ideal way of not only demodulating but of separating the users. It is necessary that uplink symbols from all users arrive at the satellite receiver in synchronism with each other and with the hop period. The Fourier transform can be performed through the chirp transform and implemented via dispersive surface acoustic wave (SAW) devices [1]. Such a processor has been implemented for demodulating multiple-user M-ary NCFSK [2]. In the present report, a demodulator is implemented using a commercially available SAW chirp transformer.

In Section 2, the measurement system is described. In particular, the SAW chirp transformer device, the methods of generating NCFSK and the jamming signals, the associated demultiplexing, the synchronization, etc., are described. In Section 3, the details of performance measurements in the presence of frequency errors, various forms of jamming, and system noise are presented. Some of the performance measurements are repeated for 3 different window functions. The conclusion is given in Section 4 and some circuit details are given in the Appendix.

2. IMPLEMENTATION

2.1 Chirp Transformer

The key component in the demodulator was the chirp SAW transformer.

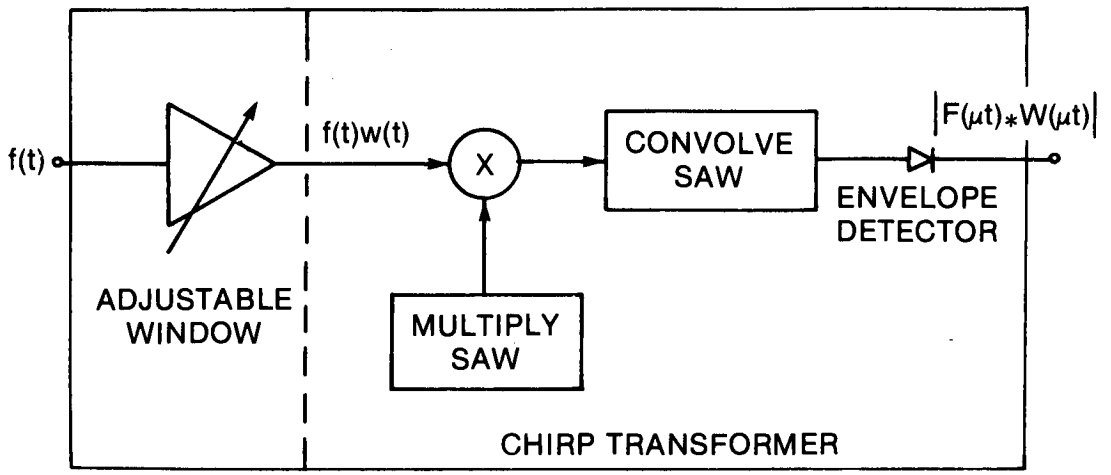

Fig. 2.1. A simplified block diagram of the RACAL-MESL SAW spectrum analyser type W1741-70.

The one used was model W1741-70 from Racal-MESL in Scotland. A simplified block diagram is shown in Fig. 2.1. The input signal f(t) was at an IF frequency of 70 MHz. The overall 1/4-dB bandwidth of the device was 4 MHz and 1-dB bandwidth was 6 MHz. An amplifier with a time varying gain impressed a time window, w(t), on the input signal. The window performed a gating function that gated out a 25 μs segment of signal for further processing every 50 μs for a 50% duty cycle. The window also provided a tapering over the 25 μs window period. This taper was adjustable from providing a rectangular 25 μs window to providing a window similar to the Kaiser-Bessel.

The 25 μs windowed signal, f(t) w(t), goes to the actual chirp transformer. The multiply-convolve-multiply format [1] was used. However, the last multiplier was omitted because its only purpose was to provide the correct phase and with noncoherent detection, phase information was not needed. The output of the envelope detector is the baseband amplitude envelope of the Fourier transform of a 25 μs segment of input signal. This spectrum analyser is an analog processor in which output time represents input frequency through a scale factor. In particular the output time, t_{out}, is related to the input frequency, f_{in}, by

$$t_{out} - t_r = (f_{in} - f_r)/\mu \qquad (2.1)$$

where μ is the chirp scale factor, t_r is a reference time, and f_r is a reference frequency. It is convenient to use offset time and frequency, $t = t_{out} - t_r$ and $f = f_{in} - f_r$, respectively so that

$$t = f/\mu. \qquad (2.2)$$

For the MESL analyser, μ = 0.16 MHz/μs. Thus, for example, a 4 MHz bandwidth at the input is displayed over a time of 25 μs on the output. The output can be written as $|F(\mu t)*W(\mu t)|$ where F(f) is the Fourier transform of f(t), W(f) is the transform of w(t), and * indicates a convolution operation.

An illustration of the timing sequence for the various operations in the MESL spectrum analyser is shown in Fig. 2.2. An input trigger pulse is repeated at the "hop" interval of 50 μs. The window starts to function about 5 μs later. For illustration, it is assumed that for the nth hop interval a CW tone of duration $\geq$ 25 μs but $\leq$ 50 μs and frequency f_n is the input to the analyser. The resulting output spectral line is located a time $(f_n - 70)/\mu$ from the location of the center frequency of 70 MHz which in turn occurs 44.525 μs after the trigger pulse. Because of this considerable delay, spectra from the nth hop will still be coming out of the analyser when the signal for the (n+1)th hop is already entering the analyser. Multiple processors would be required to achieve a 100% duty cycle.

2.2 General Description of Measurement System

A simplified block diagram of the complete measurement system is shown in Fig. 2.3. It is divided into 3 sections representing 3 components of a communication system which are: the earth terminal modulator, the channel, and the onboard demodulator.

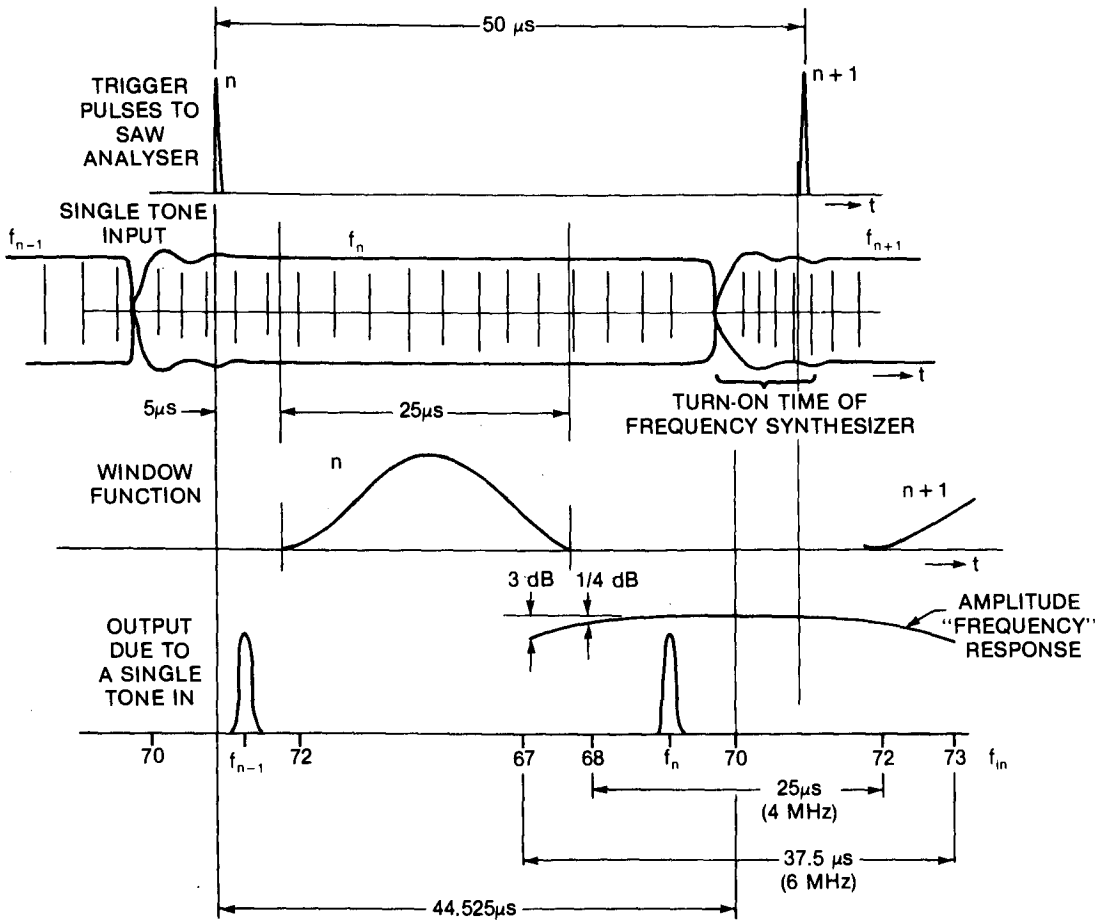

Fig. 2.2. An illustration of the timing sequence of trigger, pulse tone, window, and output signal for the MESL SAW spectrum analyser.

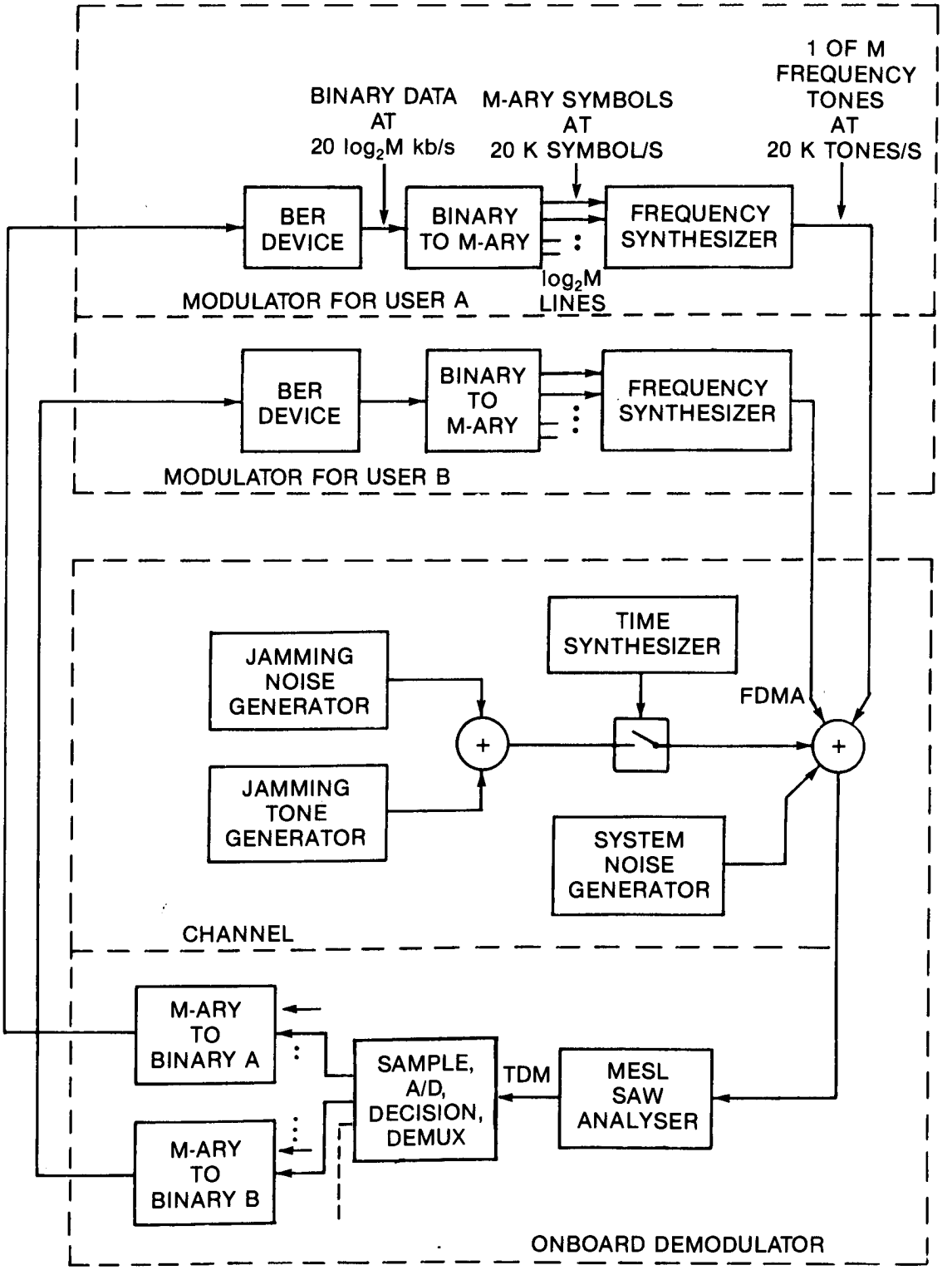

Fig. 2.3. A simplified block diagram of the multiple-user M-ary NCFSK measurement system.

A modulator consisted of a data bit generator, denoted as a "BER device", a binary to M-ary converter and a frequency synthesizer. Future low data-rate Milsatcom systems using frequency hopping (FH) will have a fixed hop rate and will be fast hopped, that is, frequency hopped at one or more hop per FSK symbol. In order to incorporate the equivalent of fast hopping in the measurement system, a symbol rate of 20k symbols/s was used in all cases to match the 50 μs "hop" interval (20k hops/s). To maintain this symbol rate, the bit rate at the BER device was 20 $\log_2 M$ kb/s. The measurement system was built to operate at selectable values of M = 4, 8, 16, or 32 which corresponds to bit rates of 40, 60, 80, 100 kb/s respectively.

The frequency synthesizer generates a new tone of about 50 μs duration every 50 μs. As illustrated in Fig. 2.2, the synthesizer has a nonzero turn-on time. However, only 25 μs of this tone is utilized so that the tone need only have a 25 μs segment of good quality. The tone has one of M frequencies as selected by the $\log_2 M$ bits fed in parallel to the frequency synthesizer. Other input lines to the synthesizer are preset to give the desired offset frequency f_0 such as illustrated in Fig. 2.4. The tone spacing used was always 100 kHz.

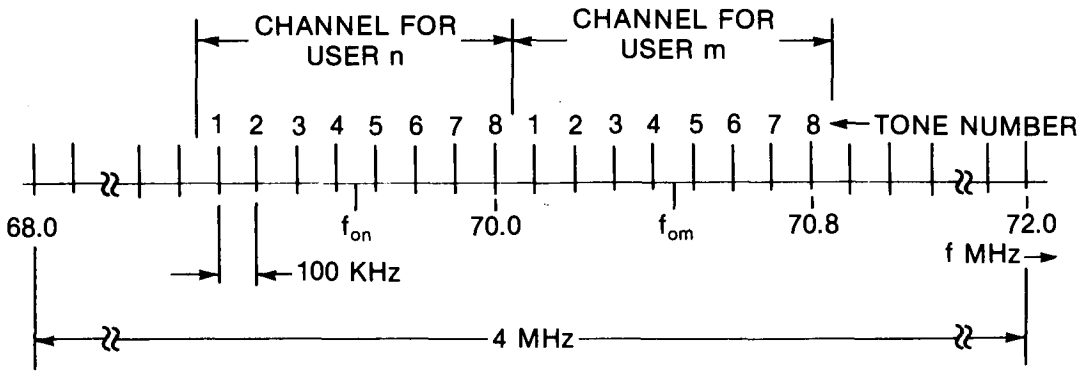

Fig. 2.4. Typical tone allocation.

Two such modulators were implemented and denoted as user A and user B. The FDMA is achieved by selecting their offset frequencies, f_{0A} and f_{0B} appropriately. The two user signals were generated in synchronism so the requirement that all user's frequency hops arrived at the satellite in synchronism to the onboard dehopper could be obeyed. The total number of tones the system can handle is 4 MHz/100kHz = 40 so up to 10 4-ary users, or 5 8-ary, and so on, or any combination, could be accommodated.

In the "channel" section, the various user signals are added together. Then jamming and system noise is added. The level of the receiver system noise generator is adjustable to provide any desired ratio of energy per symbol to noise-power spectral density, E_S/N_0. Both noise and tone jamming could be added with a selectable value of E_S/J_0 where J_0 is the power spectral density of the noise jamming or is an equivalent spectral density for multiple-tone jamming (see Sec. 3.5).

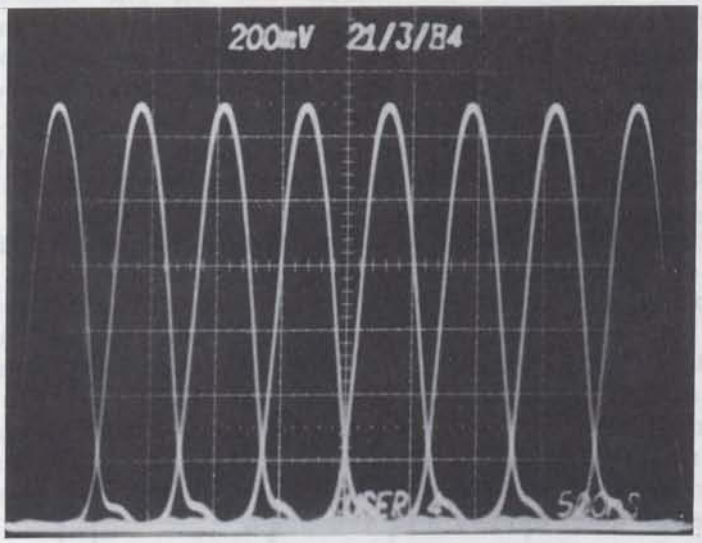

Fig. 2.5. The output of spectrum analyser for an input 8-ary symbol sequence and using nearly full windowing. The horizontal scale is 0.5 μs/div.

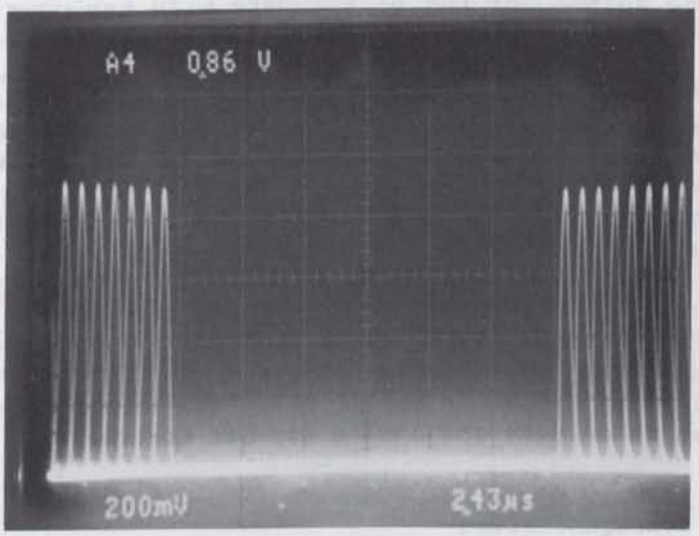

Fig. 2.6. The output of spectrum analyser for two 8-ary users with the first one in user location no. 1 and the second in user location no. 5 (Horizontal scale = 2.43 μs/div.). The first tone of user no. 1 was not displayed. Nearly full windowing was used.

In this work, single symbol 50 μs hop operation was considered only. Since the project was meant to concentrate on the demodulator, it was decided to avoid the practical difficulties of actually implementing fast hopping and dehopping. The signal at the demodulator input was made to have the characteristics of a signal that had been fast hopped and dehopped without actually hopping and dehopping by doing two things. First, each 50 μs tone burst or "hop" was generated with a phase that is independent of the phase of previous hops. This non-coherency arises naturally in the method of generating the M signal tones because the frequency synthesizer is switched to generate a new frequency tone every 50 μs without any method of maintaining phase coherence. Results of section 3.4 show that indeed the tones are noncoherent "hop-to-hop". The second technique to ensure the equivalence to a true hopping system is the method of implementing partial-band-noise (PBN) jamming or multiple-tone (MT) jamming. In an actual hopped milsatcom system, a fraction $0<\rho\leq 1$ of the hops might be jammed. This condition can be simulated without actually hopping merely by switching the jamming signal on (see Fig. 2.3) for only a fraction ρ of the "hops". The performance measured should then be exactly the same as if the signal had actually been hopped and dehopped.

The demodulator has three main components as shown in Fig. 2.3. A typical output of the spectrum analyser for a single 8-ary user is shown in Fig. 2.5. It is a time exposure with all 8 symbols being equally probable. If only a single symbol period had been pictured, then only a single tone would be seen. The input 100-kHz tone spacing results in the output spacing of $0.1/0.16 = 0.625$ μs seen in Fig. 2.5. A second example is shown in Fig. 2.6 and shows the output for two 8-ary users with one user in the first 8 slots and the second in the last 8 slots of the 40 available slots.

During every "hop" i.e. on every symbol transmitted the output of the spectrum analyser was sampled in real time exactly at the center of each of the 40 tones so that the sample spacing was 625 ns. Each sample went through an analog-to-digital conversion. The M samples for the first user channel are compared and it is decided that the symbol received is the one corresponding to the slot with the largest sample value (select largest of). This hard decision process is then repeated for the second user and so on up to 40/M users. The number of users and the value of M required is hand set in this simple measurement system. The user symbols are demultiplexed and then converted to $\log_2 M$ bits. This whole process is repeated on each 50 μs symbol or hop period. The output data is fed back to the BER device which detects and counts any bit errors.

2.3 Timing and Synchronization

Because the receiver and transmitter are co-located, normal symbol synchronization is not required. Nonetheless, considerable effort was needed to achieve proper timing of all the components principally because of the signal delays involved in the SAW analyser as illustrated in Fig. 2.2.

A simplified block diagram of the timing system is shown in Fig. 2.7. More detailed circuit diagrams are given in the appendix. All timing is run from a 19.2 MHz master clock. The BER data generator is clocked by a 40, 60, or 80 kHz clock signal for M=4, 8, or 16 respectively. The synthesizer

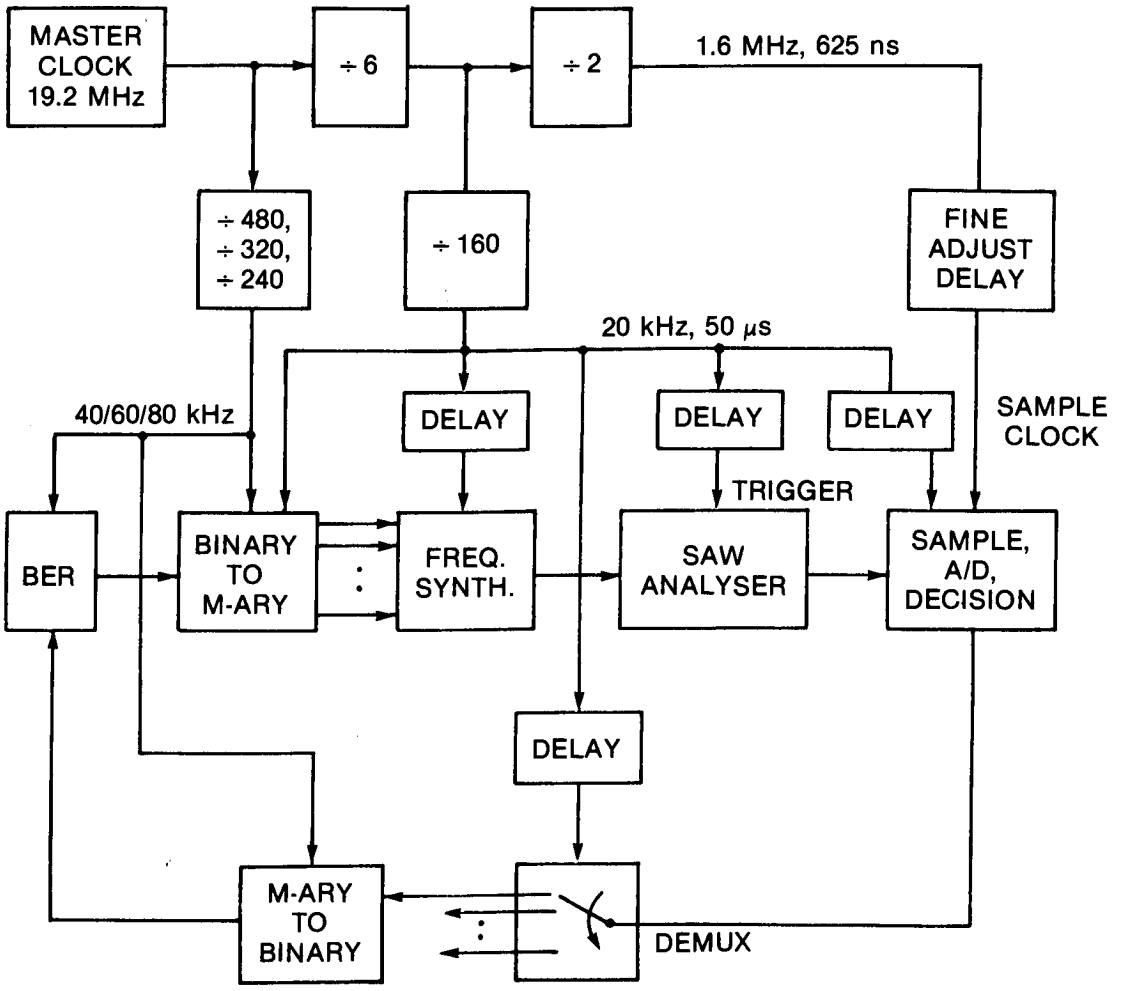

Fig. 2.7. A simplified timing block diagram.

and the SAW analyser are both clocked at 20 kHz. The sampler for the A/D is operated at 1.6M samples/s with a sample spacing of 625 ns.

Various digital "delays" are used for a variety of reasons. The delays in the 20-kHz clock to the synthesizer and the SAW analyser are to compensate for the fact that both the window function and the output of the SAW analyser are delayed relative to the input trigger time, as illustrated in Fig. 2.2. There was a fine adjust delay for the clock to the sampler to ensure that the samples were taken exactly at the center of each 625 ns tone slot (representing 100-kHz tone spacing). For the decision device and the demultiplexer it was necessary to set counters so as to ensure each user was operated for exactly the correct value of M samples and then reset for the next user's signal.

3. MEASUREMENTS

3.1 SAW Analyser

In this subsection measurements on some of the important characteristics of the MESL spectrum analyser are presented. In particular, topics covered are: nonlinearity of the amplitude response, window shape, and the effect of windowing on sidelobes.

There is some nonlinearity in the analyser probably arising mostly from the envelope detector at the output. It is assumed that the output envelope voltage V_0 is related to the input RF voltage V_i by

$$V_0 = c_1 V_i^{\,p} \tag{3.1}$$

where c_1 is a constant and p the value of the power law being measured. By taking $20\log_{10}$ of both sides we get

$$20\log_{10} V_0 = p[10\log_{10} P_i] + c_2 \tag{3.2}$$

where $10\log_{10} P_i$ is the input RF power in dBm and c_2 is a constant. The measured values of $20\log_{10} V_0$ are plotted against the input power in dBm in Fig. 3.1. The operating RF frequency was 70 MHz. The maximum permissible input of 0 dBm results in V_0=2.1V. The slope of the curve is p. At high input levels p≈1/2 and there is compression of the output. At the middle of the operating range, p≈1, corresponding to linear operation. As the input decreases to its lowest value, p≈1.5 which is approaching square-law operation. The nonlinearities occur only at the upper and lower ends of the operating range and are only modest nonlinearities. They should have relatively little effect upon error performance especially since the analyser was operated in the linear region for most performance measurements.

The ratio of the maximum permissible output of 2.1V to the minimum detectable output was found to be about 50 dB. This agreed with the manufacturer's value of noise-limited dynamic range.

To achieve the window, a variable gain amplifier was used. The voltage waveform shown in Fig. 3.2 is used to vary the amplifier's gain. It has a

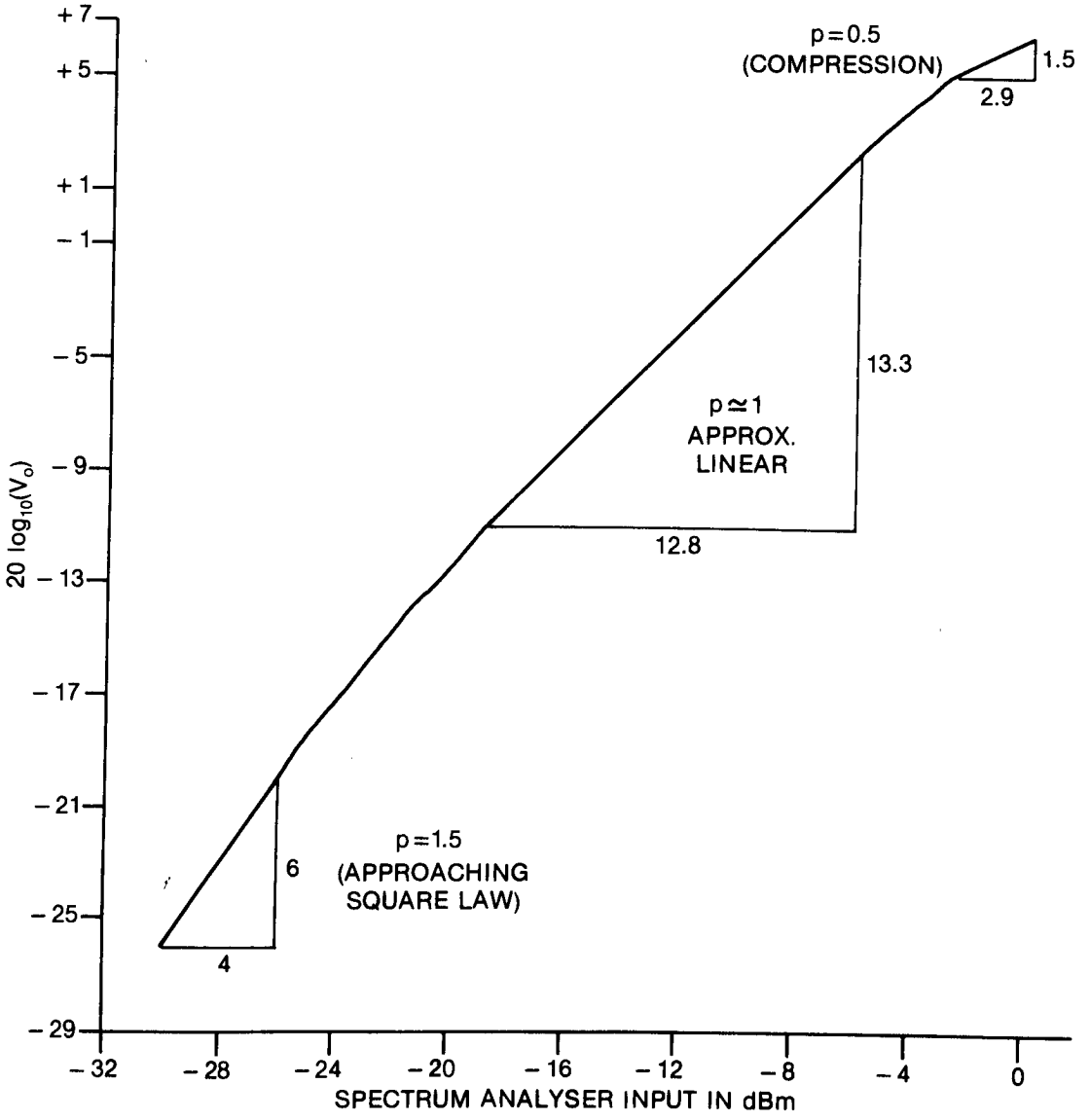

Fig. 3.1. Measured values of 20 log V_0 versus input RF power in dBm for the MESL spectrum analyser.

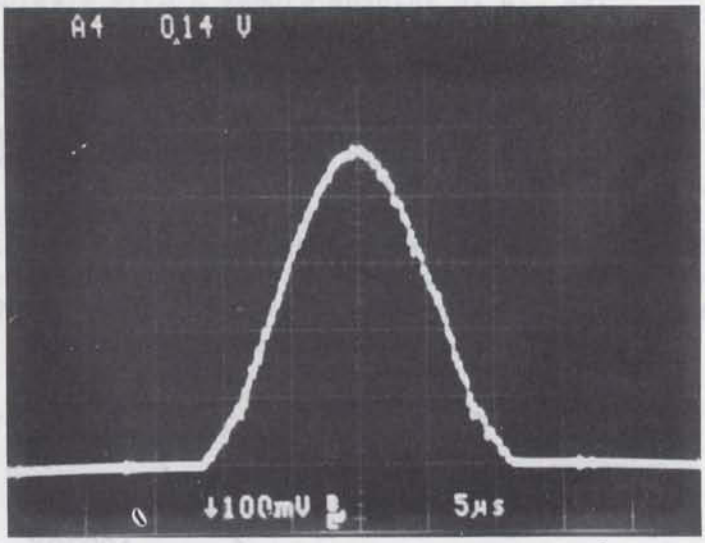

Fig. 3.2. The control voltage for the variable gain amplifier. Horizontal scale is 5 µs/division. The vertical scale is linear in volts.

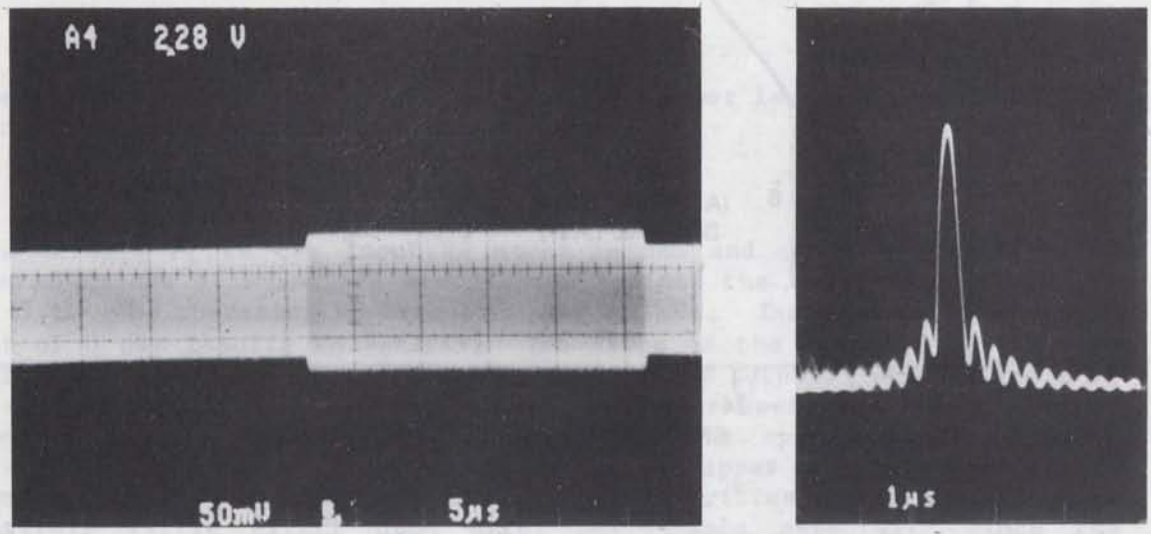

(a) (b)

Fig. 3.3. The waveforms for a rectangular window with (a) the windowed input IF voltage (5 µs/div) and (b) the output voltage for a single input tone (1 µs/div). The vertical scale in (a) is linear in volts and in (b) is linear amplitude of the Fourier transform.

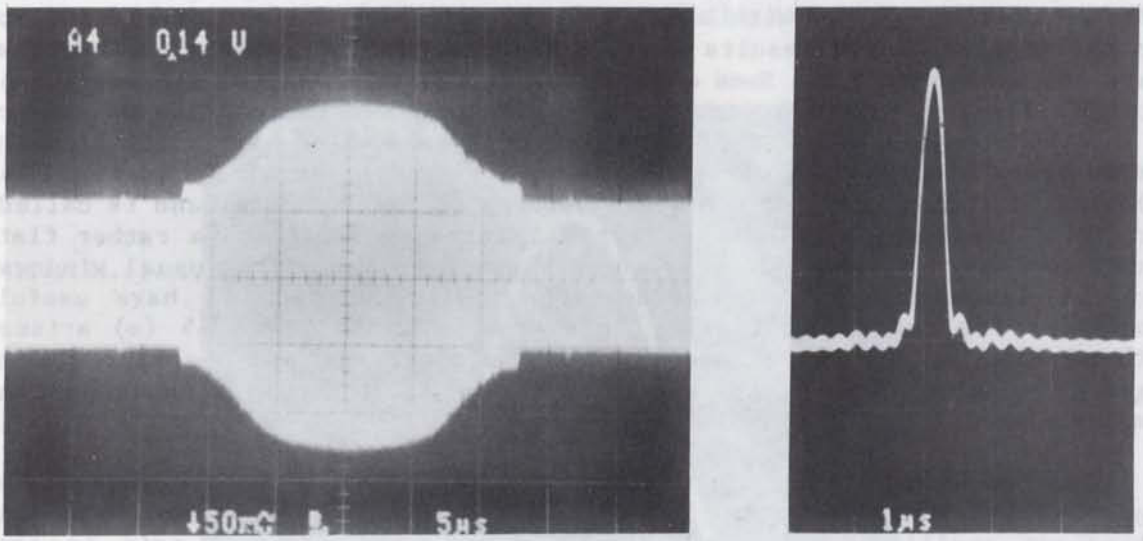

(a) (b)

Fig. 3.4. The waveforms for an "intermediate" window with (a) the windowed input IF voltage (5μs/div), and (b) the output voltage for a single input tone (1 μs/div). The vertical scales are linear as in Fig. 3.3.

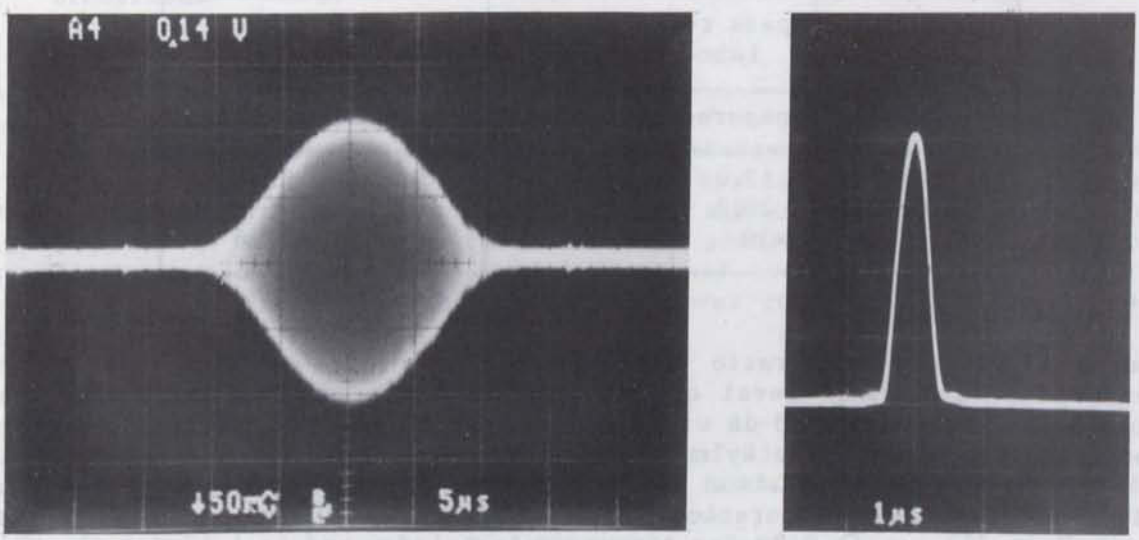

(a) (b)

Fig. 3.5. The waveforms for "full" windowing with (a) the windowed input IF voltage (5 μs/div) and (b) the output voltage for a single input tone (1 μs/div). The vertical scales are linear as in Fig. 3.3.

width of 25 μs. A potentiometer adjustment controls a bias that can be added to this waveform. With a large bias, the taper disappears and a flat top rectangular window results whereas with no bias the window follows the shape shown in Fig. 3.2. Some examples of the IF signal after windowing are shown in Figs. 3.3 (a) through 3.5 (a). The signal seen outside the basic 25 μs window region consists of out of band signals which has no effect upon the analyser's output and can therefore be ignored. The window in Fig. 3.4 (a) results from a bias set somewhere between full and no bias and is called here an "intermediate" window. It has a large pedestal and a rather flat center section. It does not seem to correspond to any of the usual windows such as listed in [3]. Nonetheless it will be seen to have useful properties for our application. The window shown in Fig. 3.5 (a) arises with no bias and is called here a "full" window. It has the approximate shape of a Kaiser-Bessel (KB) window with $\alpha \approx 1.6$ but many windows have a similar shape.

The resulting output spectrum for a single CW tone input is shown in Figs. 3.3 (b) through 3.5 (b) for the 3 windows. In these Figs. and all subsequent oscilloscope traces of the output, the vertical axis is the amplitude of the Fourier transform and is linear in scale. From these, the

Table 3.1

Values of peak-to-sidelobe ratio and 3 dB width for the 3 windows used.

window	peak to first side lobe ratio, dB		3-dB width, kHz	
	measured	theoretical	measured	theoretical
rectangular	12.0	13	36	35.6
intermediate	20.2	--	48	----
full	≈30	37	65	52.8

peak-to-first-side-lobe ratio was measured as well as the 3-dB width (measured at the 0.707 level of the peak) and the results are listed in Table 3.1. The measured 3-dB width was converted from the time value to the equivalent frequency value by multiplying by μ=0.16 MHz/μs. The theoretical sidelobe levels obtained from [3] are listed for the rectangular and KB, α=1.6, windows. The theoretical 3-dB width is calculated from c_1/T MHz where, from [3], c_1 is 0.89 for a rectangular window and is 1.33 for the KB, α=1.6 window; and T=25 μs.

For the rectangular window, the measured sidelobe ratio and the 3-dB width are very close to the theoretical. For the full window, the measured sidelobe ratio was 7 dB less than theoretical and, as can be seen in Fig. 3.6, was unsymmetrical. The manufacturer claimed a sidelobe level of -40 dB whereas we measured a level of -30 dB. This larger than expected sidelobe level degrades the tolerance to interchannel interference. It was suspected that the SAW devices in the spectrum analyser had phase slope mismatch leading to larger sidelobes than theoretically predicted. The measured 3-dB

bandwidth was slightly wider than theoretical. For the intermediate window the measured parameters fall between those of the other 2 windows as might be expected.

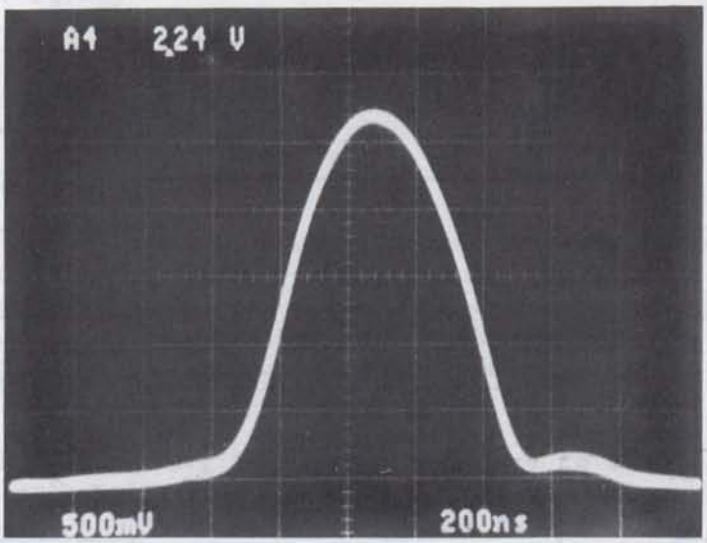

Fig. 3.6. An expanded view of Fig. 3.5 (b), the output of the spectrum analyser for a single tone with "full" windowing. The horizontal scale is 200 ns/div. and the vertical axis is linear in amplitude of the transform.

3.2 Measurements with System Noise

The first performance tests made were measurement of bit-error rate as a function of system noise. The measurement system shown in Fig. 2.3 was used. It is shown in Fig. 3.7 where the power measurements were taken. The signal power C is measured with an average power meter. The switching transients as the synthesizer changed frequency every 50 μs were found to have negligible effect upon the average IF power reading. The energy per symbol, E_s, was calculated as

$$E_s = C \times 25 \times 10^{-6} \text{ joules} \qquad (3.3)$$

where C is in watts. The basic symbol length of 25 μs is thereby accounted for and the actual repetition or "hop" period (usually 50 μs) has no effect on the results. The total average noise power, N, passing through the bandpass filter is measured. The effective noise bandwidth of the filter was accurately measured as 9.86 MHz. Thus the noise power spectral density is calculated from N by

$$N_0 = N/9.86 \times 10^6 \text{ W/Hz}. \qquad (3.4)$$

Thus, the desired ratio of E_s/N_0 is calculated from the measured values of C and N by

$$E_s/N_0\big|_{dB} = C\big|_{dBm} - N\big|_{dBm} + 10\log(25 \times 9.86). \qquad (3.5)$$

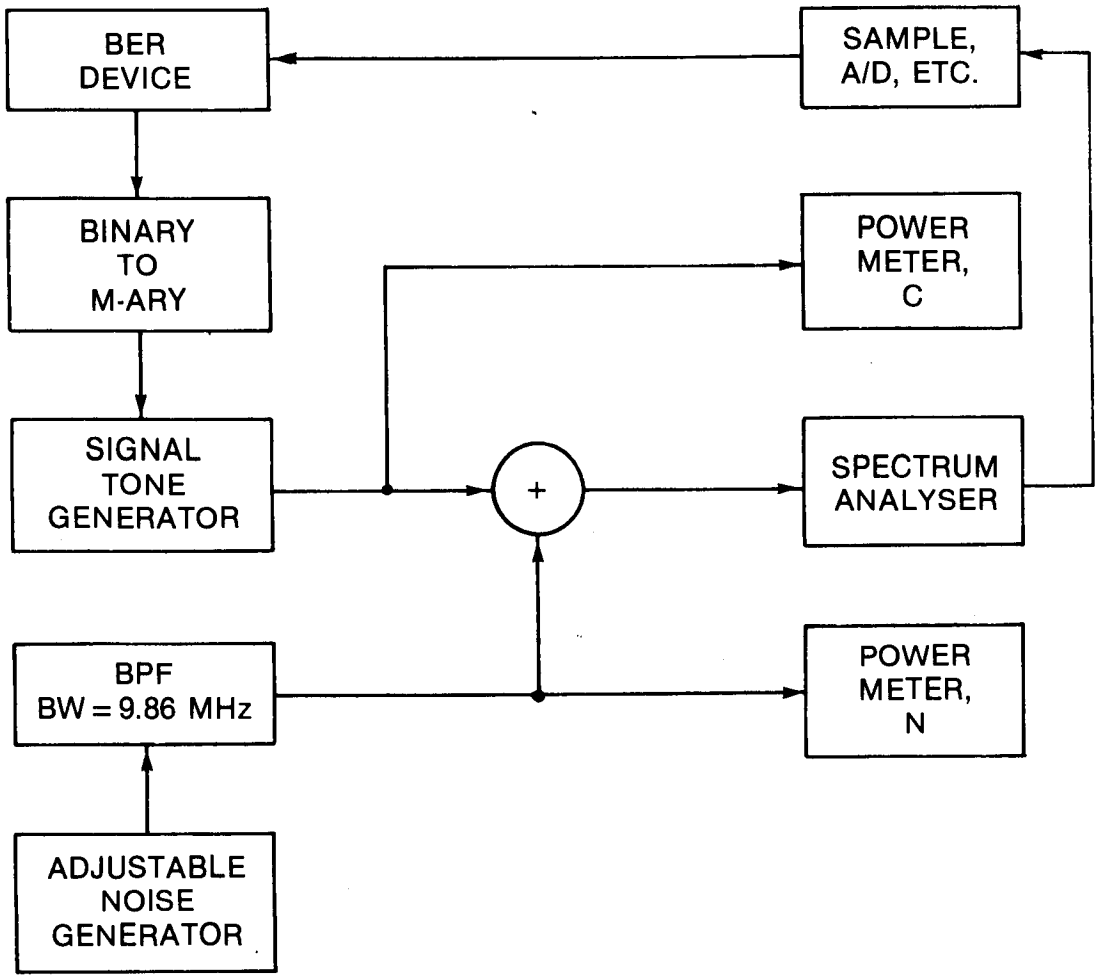

Fig. 3.7. A simplified block diagram of the performance measurement system for measuring bit-error rate as a function of C/N_0.

The probability of bit error for M-ary NCFSK in the presence of gaussian noise of double-sided density $N_0/2$ W/Hz is [4]

$$P_b = \frac{\exp(-E_s/N_0)}{2(M-1)} \cdot \sum_{j=2}^{M} (-1)^j \binom{M}{j} \exp(E_s/jN_0). \qquad (3.6)$$

In Fig. 3.8 the results of measurements for 8-ary FSK are shown where a curve is given for each of the 3 windows discussed in Sec. 3.1. Values of P_b greater than about 0.05 were not obtained because the BER device yields inaccurate results in this region. For P_b below 10^{-6}, it took too long to obtain statistically meaningful error counts so these values were not measured either.

In such a demodulator, two losses relative to the theoretical arise. One is the implementation loss and the other is the window loss. The window loss is related to the loss in energy caused by the window and is measured relative to a rectangular window. In [5] the window loss is shown to equal 10log of the equivalent noise bandwidth (ENBW) tabulated in [3]. Thus, the window loss of the reference rectangular window is 0 dB, and for the KB, α = 1.6 window, the window loss is 1.37 dB.

For the rectangular window it is seen that the implementation loss goes from about 0.4 dB for large P_b to about 0.6 dB at low P_b with a mid-range loss of about 0.5 dB. Such a low implementation loss is considered as very good. The loss gets larger with decreasing P_b probably because the internal noise of the analyser is having more of an effect.

For the full window, the loss from theoretical at mid range is about 1.9 dB. If the implementation loss of 0.5 dB is removed there remains a window loss of 1.4 dB which is very close to the theoretically predicted value of 1.37 dB. For the intermediate window a total mid range loss of about 0.8 dB is measured which corresponds to a window loss of about only 0.3 dB.

Measurements of P_b for 4-ary and 16-ary were also taken but only for the intermediate window. The results are shown in Figs. 3.9 and 3.10. Combined implementation plus window losses are about 0.65 dB and 0.8 dB for the 4-ary and 16-ary respectively. The difference of 0.15 dB in combined loss is probably within the measurement accuracy.

3.3 Measurements with Frequency Errors

In a real satellite system, the dehopped tone will have some frequency error, relative to its corresponding onboard frequency slot. In this section the degradation in performance caused by such frequency errors is considered.

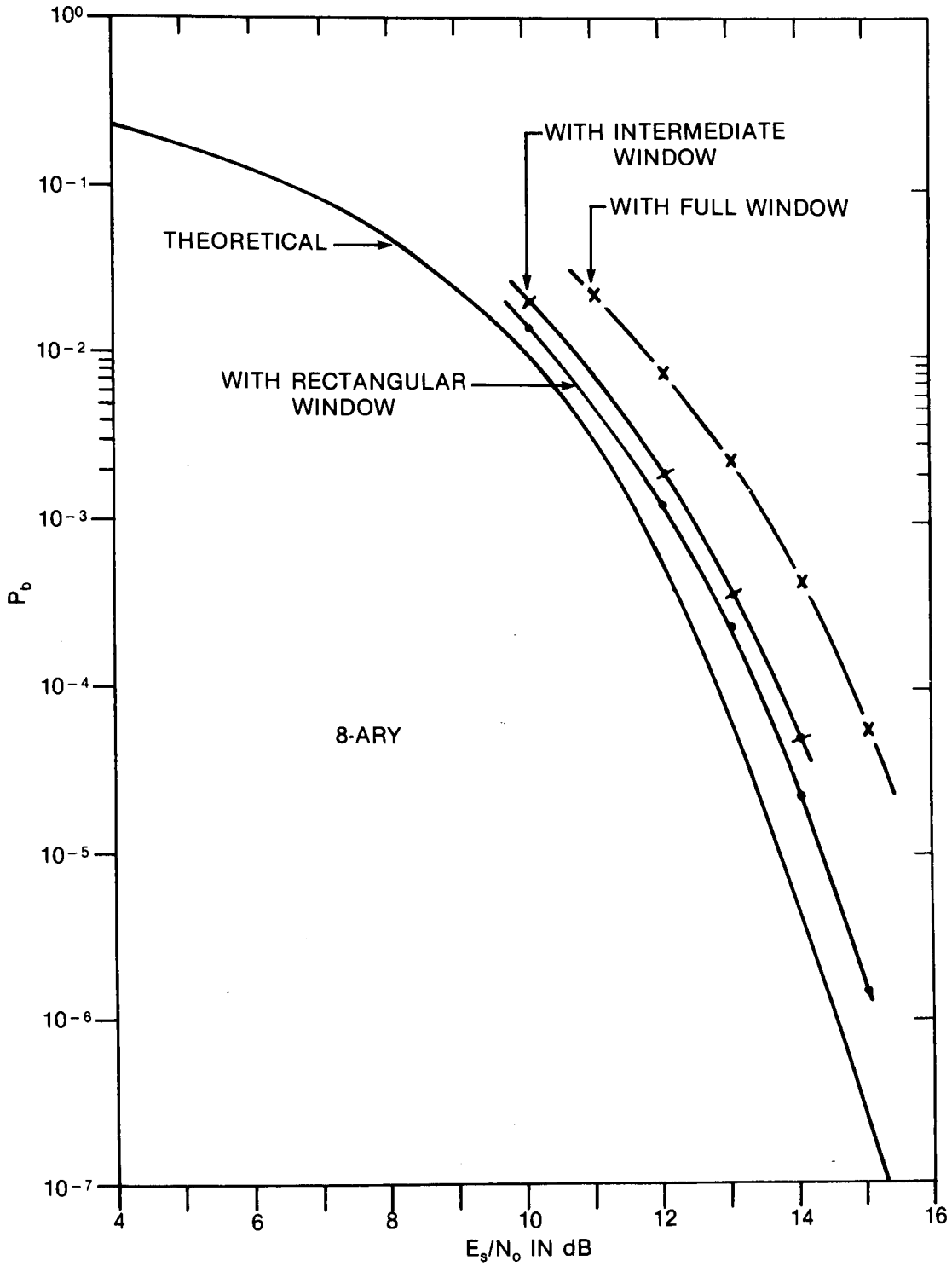

Fig. 3.8. The bit error rate measured for 8-ary FSK with three different windows.

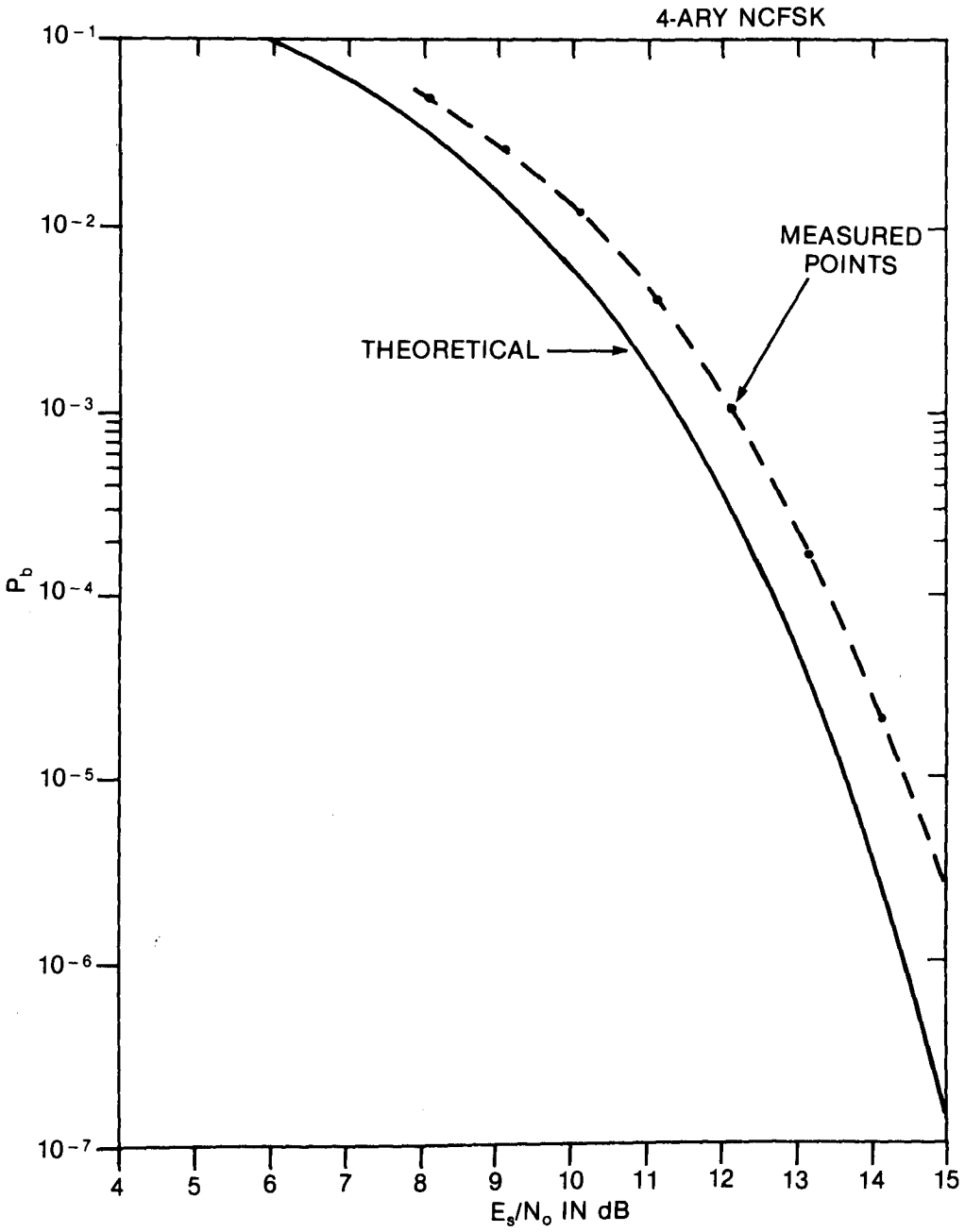

Fig. 3.9. The bit error rate measured for 4-ary FSK with an intermediate window.

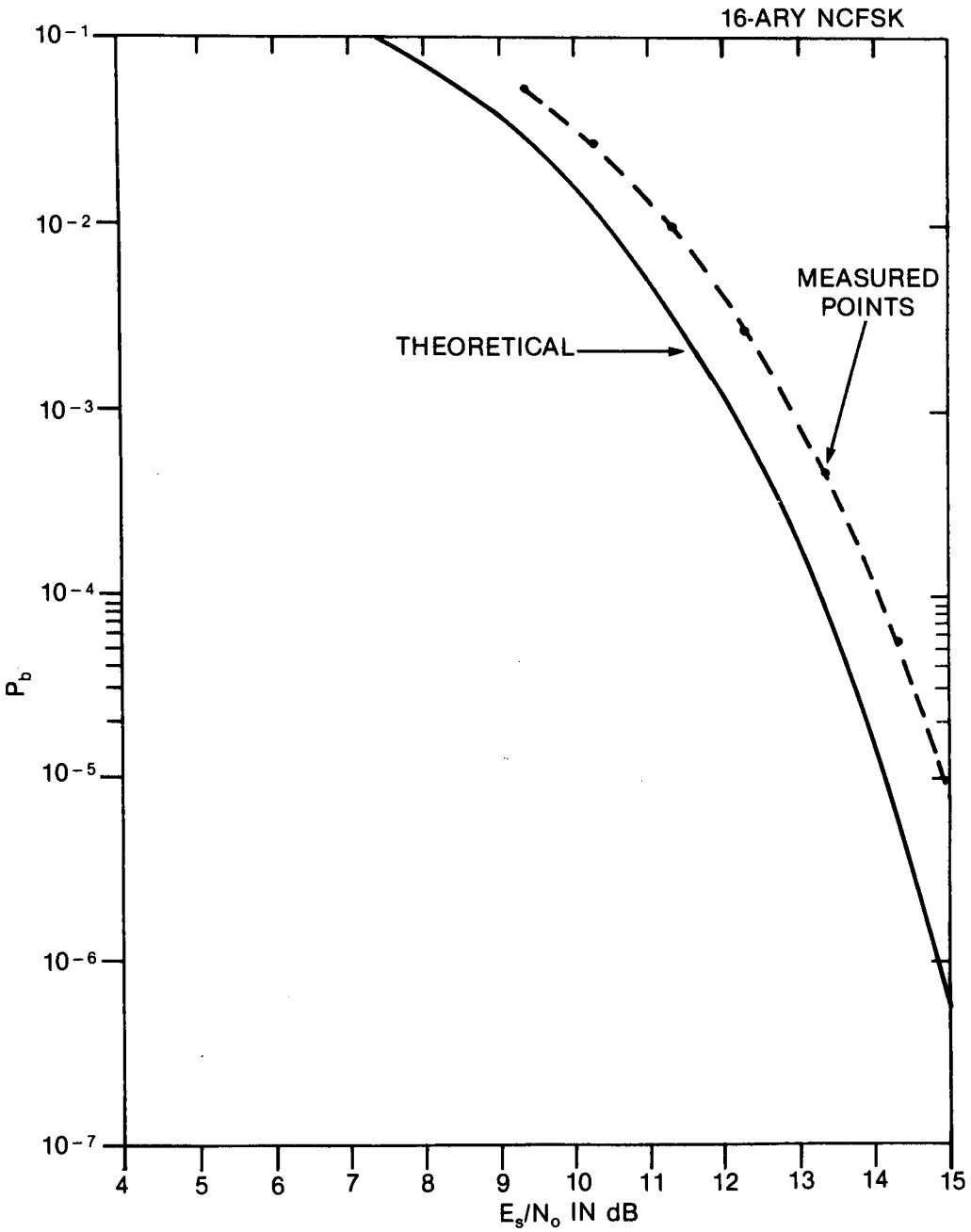

Fig. 3.10. The bit error rate measured for 16-ary FSK with an intermediate window.

It is noted that for orthogonal tone spacing the tones are separated by N/T where N=1,2,... Since here T=25 μs, the minimum orthogonal spacing is 40 kHz. The actual time spacing used was 100 kHz for the convenience of the circuitry. This separation is 2 1/2 times the minimum orthogonal spacing whereas systems that use non-rectangular windows normally use separations of no more than about twice the minimum orthogonal so as to achieve a good trade off between bandwidth efficiency and error performance.

In order to measure the effects of frequency errors, the tones generated by the frequency synthesizer shown in Fig. 2.3 was offset by a constant amount for all FSK symbols. Frequency offsets of 10 kHz and 20 kHz, which correspond to shifts of 10% and 20%, respectively, of the 100 kHz tone spacing, were used. For both of these frequency errors, the 3 windows, rectangular, intermediate, and full, were used.

The results of the measurements are shown in Fig. 3.11. Only 8-ary FSK was studied. These curves can be compared to those for no frequency error in Fig. 3.8. The shift of the curve at $P_b = 10^{-3}$ due to frequency error is listed in Table 3.2. In columns A is the combined loss due to implementation, windowing, and frequency error. In columns B, the losses due to implementation and windowing have been removed leaving only the loss due to frequency error.

Table 3.2

The degradation in performance in dB caused by frequency errors for the 3 windows at $P_b = 10^{-3}$.

Freq. Error / Window	10 kHz		20 kHz	
	A	B	A	B
Rectangular	1.4	1.0	4.6	4.2
Intermediate	1.4	0.6	3.6	2.8
Full	2.2	0.4	3.4	1.5

A is the offset in dB from the theoretical curve for a rectangular window and is the sum of implementation, window, and frequency error losses.

B is the loss in dB due to frequency error alone.

For a 10 kHz shift, which is a moderately large frequency error, relatively little loss occurred. The rectangular and the intermediate window out performed the full window because the frequency error losses are less than the window loss of the full window. For a large frequency error of 20%, the frequency error losses begin to be significant. The full window finally out performs the rectangular window. The intermediate window is seen to perform almost as well as the full window.

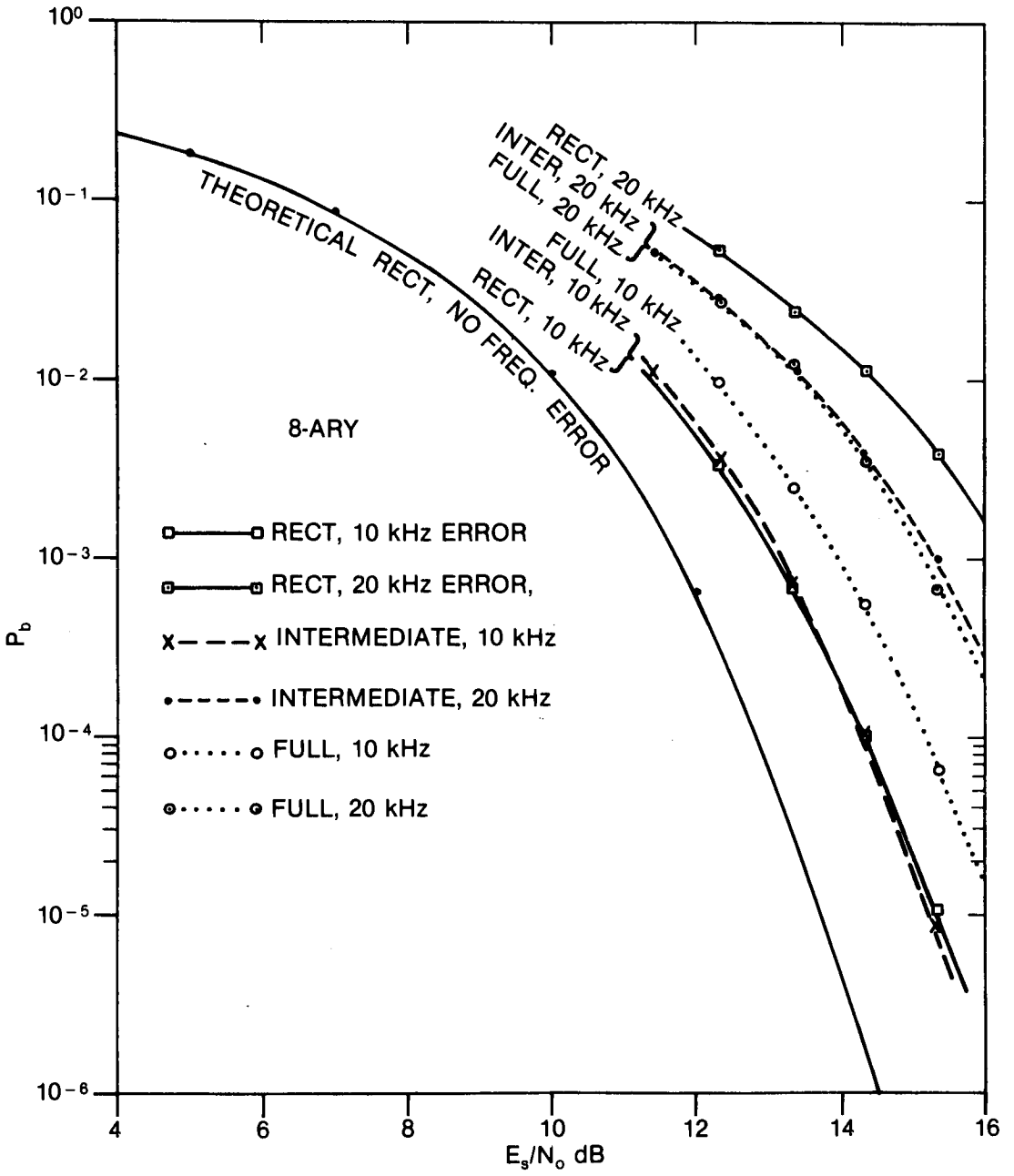

Fig. 3.11. Bit-error rate for 8-ary FSK for frequency errors of 10 kHz and 20 kHz for 3 windows.

(a)

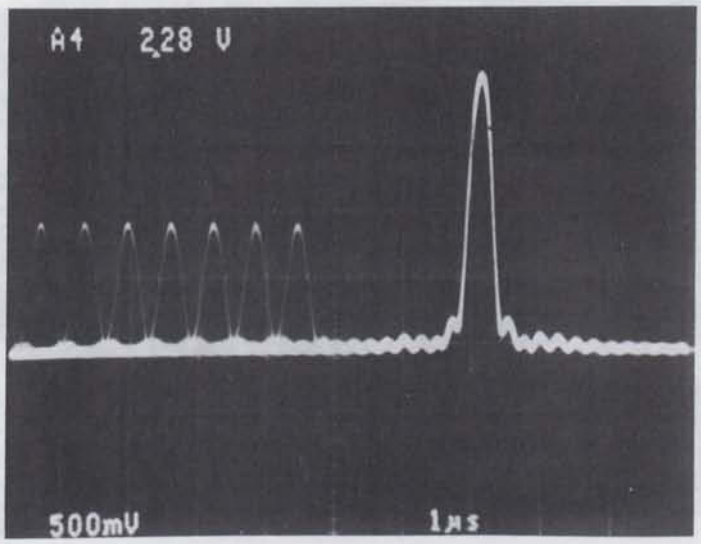

(b)

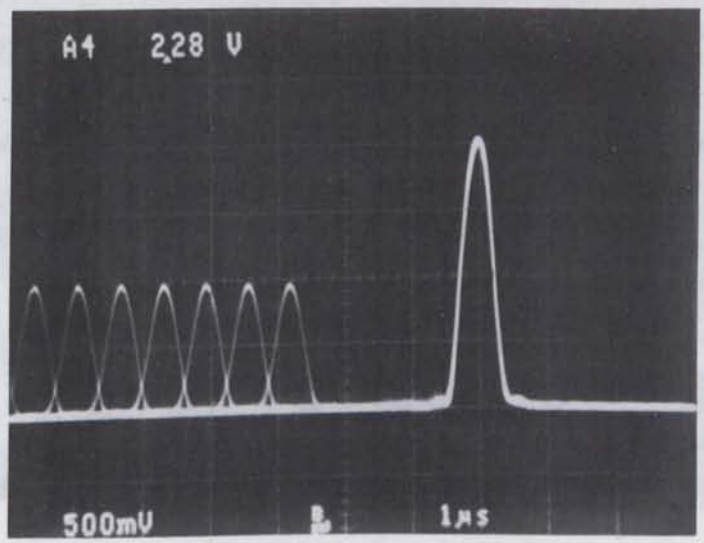

Fig. 3.12. Output of the spectrum analyser for an 8-ary input signal plus an interfering tone with (a) using an intermediate window and (b) using a full window. Horizontal scale is 1 μs/div.

(a)

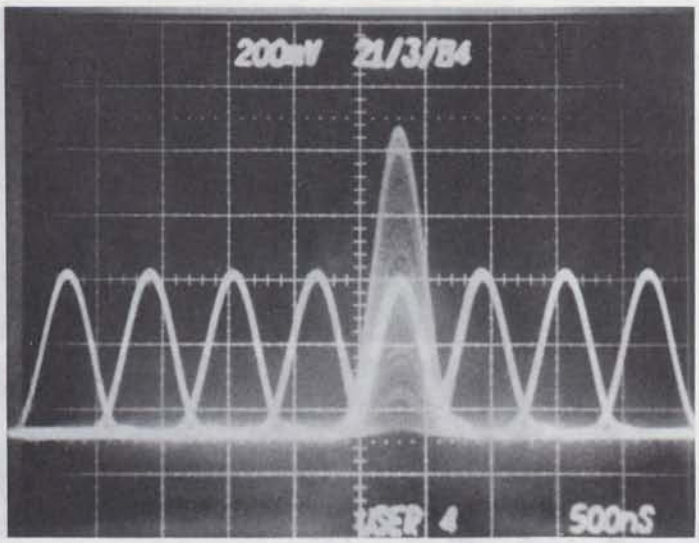

(b)

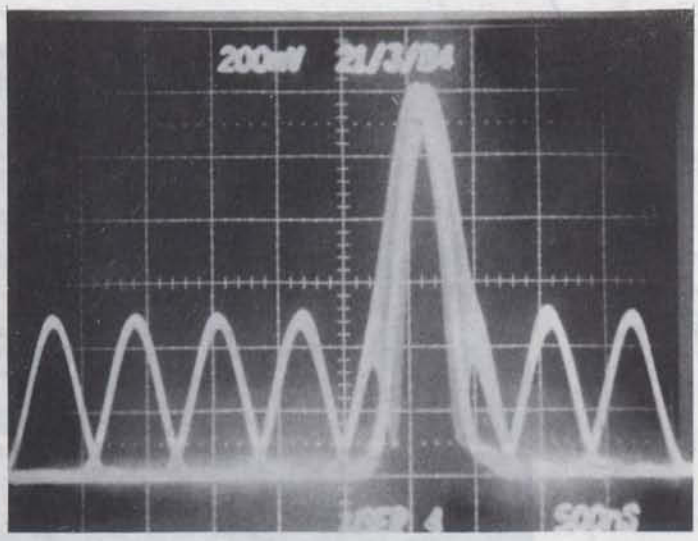

Fig. 3.13. The output of the spectrum analyser for an 8-ary input signal plus an interfering tone (a) of equal amplitude located exactly on the 5th signal tone location and (b) of larger amplitude and located exactly between 2 signal tone locations. A nearly full window was used.

(a)

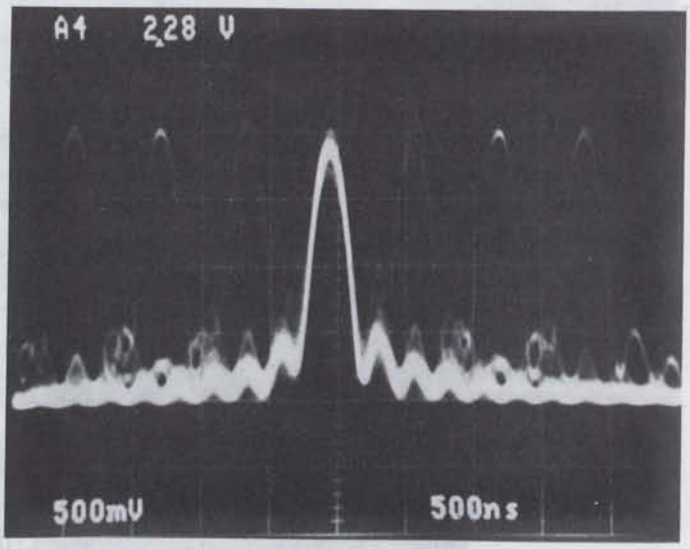

(b)

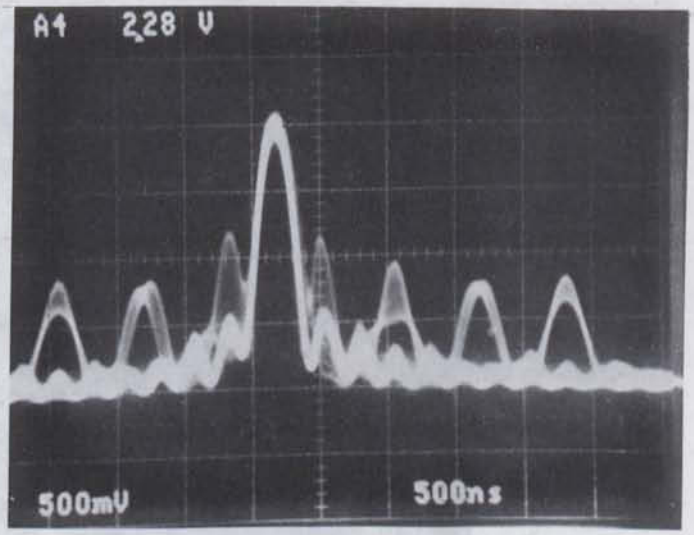

Fig. 3.14. As in Fig. 3.13 but with a rectangular window.

(a)

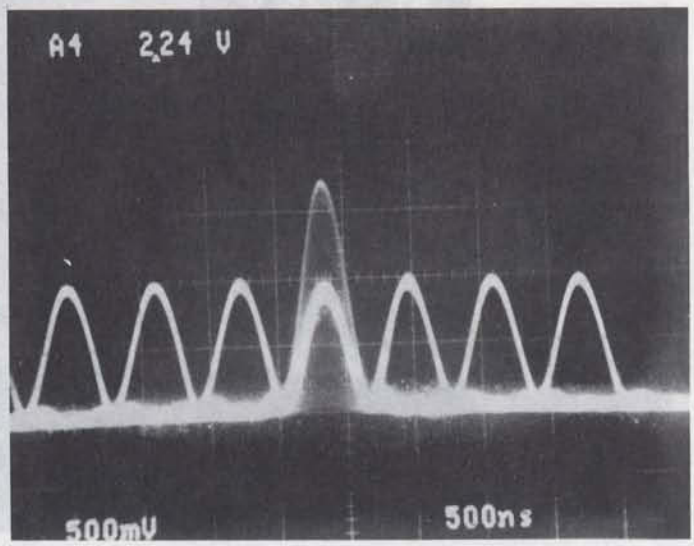

(b)

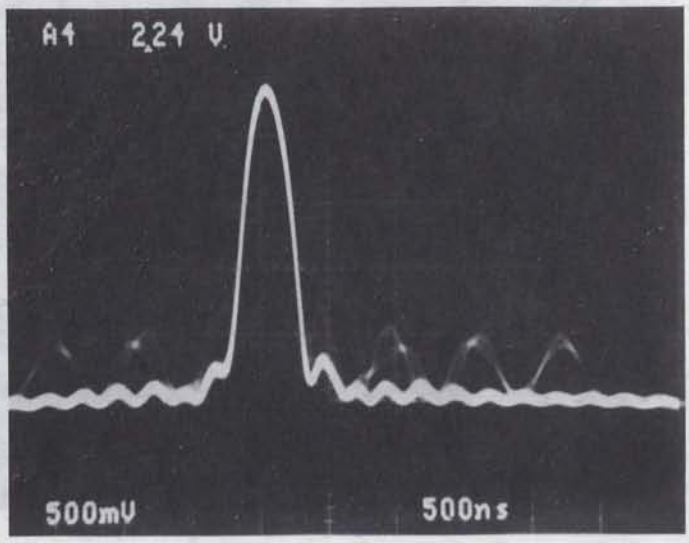

Fig. 3.15. As in fig. 3.13 but with an intermediate window.

(a)

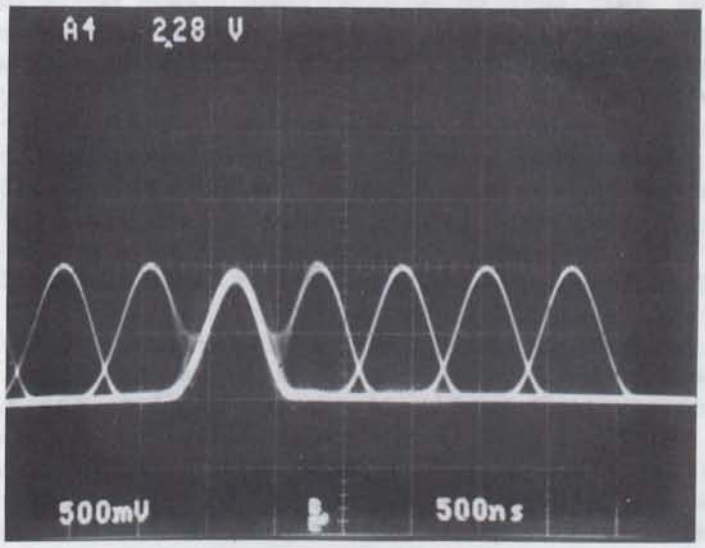

(b)

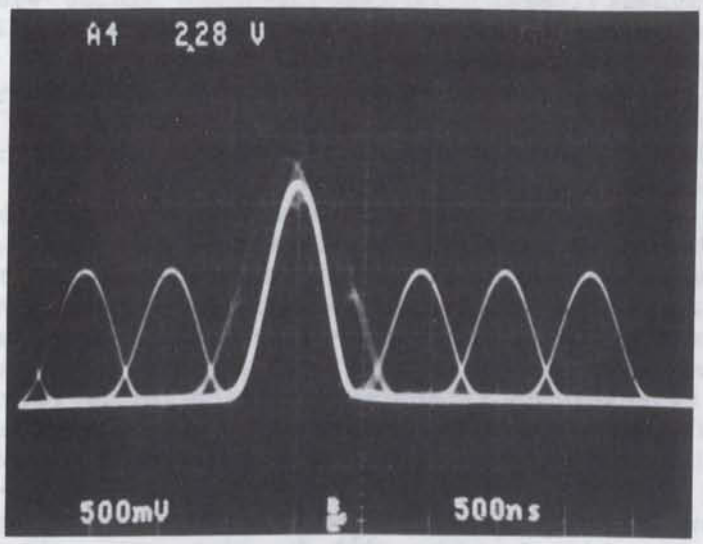

Fig. 3.16. As in Fig. 3.13 but with a full window.

It is concluded that if the worst expected frequency error is 10% then rectangular or intermediate windows would be recommended. For large frequency errors of 20% then system performance is poor with any window but with intermediate and full windows performing slightly better than rectangular windows.

Initial theoretical analysis of the effects of frequency errors on performance are found in [6]. Further analysis is currently under way.

3.4 Interfering Tone Location and Adjacent Channel Interference

In this subsection, the effects of interfering tones located in or near a user's channel are considered. As shown in Figs. 3.12, a tone of adjustable position and amplitude can be added to the desired signal. In these Figs., 8-ary FSK symbols are used. Only 7 of them are visible on the photos. The interfering tone appears much brighter than the 8-ary signal tones because the interference is present at one location during all 25 μs symbol periods whereas a particular signal tone is present, on the average, on 1/8 of the symbol periods. Thus, the signal tones get about 1/8 the exposure that the interfering tone does. In the following, the tone is moved to a number of locations to study its effect.

In Fig. 3.13 (a) through 3.16 (a), the interfering tone is placed exactly on one of the signal tone locations and has an amplitude close to that of the signal tones. In Fig. 3.13 the window was nearly the full window. Rectangular, intermediate, and full window were employed for Figs. 3.14, 3.15, and 3.16 respectively. All 8 tones are in view in Fig. 3.13 whereas the first signal tone is out of view in the remaining Figs.

Fig. 3.13 (a) perhaps is the clearest in showing how the signal and interfering tones combine. Because the signal tone is generated by switching on a frequency synthesizer for every new symbol, the signal's phase is different on each symbol relative to the phase of the interfering tone which is on continuously. Thus, the combined amplitude can be seen in Fig. 3.13 to be as much as twice the individual amplitudes, indicating that the signals are adding in phase, or are of about zero amplitude indicating complete cancellation. Over many symbol periods it is seen that the range between the two extremes is approximately uniformly filled indicating that the phase of the signals tones are uniformly distributed. This phase distribution shows that indeed the FSK signals were noncoherent.

In Figs. 3.13 (b) through 3.16(b), the interfering tone is somewhat larger than the signal tones and is placed exactly between two tone locations. Perhaps the clearest photo for illustrating the effects is in Fig. 3.13 (b). Again, the desired and interfering signals combine constructively or destructively depending upon their relative phases. The sample points are not at the peak of the interference but are on both sides of it. Therefore interfering tones located between signal tone locations must be large before errors start to occur.

The effect of an interfering tone depends on its location and amplitude relative to the user tone positions. From the communicator's view point the worst place an interfering tone can be is exactly on one of the user's M

tones; the location within the user's channel that causes the least performance degradation is exactly half way between 2 tone locations. A tone was placed in these positions and its amplitude increased until the occasional error started to occur. The results are listed in Table 3.3. As expected, for the interfering tone exactly on a signal tone, the interference must be increased to almost equal the signal before any errors occur. The reason errors occur before the amplitude are equal (0 dB) is that the small amount of internal system noise can add to the interference or subtract from the signal to cause an error. With the tone between 2 signal tones the intermediate window gives by far the best protection. Interestingly, the full window gives the decidedly worst performance which likely arises from the fact that the spectral line for the full window is somewhat wider than the others and therefore it's sides spill into adjacent slots more than for the other.

Table 3.3

The ratio of the minimum interfering tone power to signal power required to cause symbol errors for 3 locations of the interfering tone

Window	Interfering tone power to signal-power ratio in dB for tone located:		
	exactly on a signal tone location	exactly between two signal tone locations	in nearest adjacent slot
Rectangular	-1 dB	+10 dB	+15 dB
Intermediate	-0.5 dB	+16 dB	+24 dB
Full	-0.5 dB	+ 5 dB	+26 dB

For multiple users, interchannel interference can become a problem especially if one user's received signal is much stronger than the received signal in an adjacent channel. To measure this effect, the interfering tone was moved to be exactly on the slot adjacent to the last slot in one user's channel. For the 8-ary FSK signals this location corresponds to what might be called the 9th slot. The interfering tone is in this slot on every "hop" whereas in an actual system it would be located in the worst slot on only 1/M of the hops. However, since we are not measuring absolute performance but merely when errors start to occur, the worst-case placement of an interfering tone on every "hop" does not affect the results. From Table 3.3 it is seen that the full window gives the best performance which is expected because the full window gives the lowest sidelobes. However, because of the large 2.5/T tone spacing, the intermediate window performs almost as well as the full window. Thus, the final selection of a window function must consider not only the side-lobe level but also the width of the main lobe.

3.5 Measurements with Partial-Band-Noise and Multiple-Tone Jamming

It is often assumed that a jammer has an average power constraint. A signal-to-jamming power ratio is defined as

$$SJR = E_s/J_0$$

where for noise jamming, J_0 is the jamming power spectral density if the total jamming power were spread uniformly across the entire hopping band. For multiple-tone jamming the meaning of J_0 is altered to mean the power in one tone if the tones were uniformly distributed across the hop band with one tone to a bin so that there would be M jamming tones in a user's channel. An intelligent jammer attempts to distribute its given power to cause the most degradation in performance. To do this, only a fraction $0 < \rho \leq 1$ of the hops are jammed but at an increased power level of J_0/ρ. On the other $1-\rho$ of the hops, no jamming is present and there is only system noise with an unjammed SNR of E_s/N_0.

Hop frequencies are generated pseudorandomly, so that the desired signal hops randomly into a jammed channel on the fraction ρ of the hops on the average. However, to simulate partial-band noise (PBN) or multiple-tone (MT) jamming it was found simpler to jam the hops on a regular basis rather than randomly. A pulse generator denoted as a "time synthesizer" in Fig. 2.3 was used to close the switch regularly for one hop out of every $1/\rho$. For example, for $\rho = 0.1$, every 10th hop was jammed. Since the outcome of one hop has no effect on any other hop, an uniform distribution of jammed channels results in the same overall symbol error rate as a random distribution.

For the measurements, a value of E_s/N_0 is set and E_s/J_0 is chosen. Then ρ is varied with a setting of the "time synthesizer". Simultaneously the jamming power is varied to be J_0/ρ. For PBN jamming, the jamming occupies the entire M x 100 kHz user band. For MT jamming, only a single tone per M x 100 kHz band was used because it has been determined [7] that this value is worst-case tone jamming. Furthermore, the jamming tone is located exactly on one of the M signal tones which is the worst-case position as seen in the previous subsection.

In Fig. 3.17 is shown the performance of 8-ary NCFSK in the presence of PBN jamming for two values of SJR. The value of $E_s/N_0 = 30$ dB was the value set by the internal noise of the chirp transformer system. The solid lines are values calculated theoretically from techniques developed in [7]. The markers are the measured values after correction for implementation loss. The measured values came very close to the theoretical values. Worst-case values of ρ are easily seen and are dependent upon SJR.

In Fig. 3.18 the performance of 8-ary NCFSK is shown in the presence of MT jamming for two values of SJR. System noise was set so that $E_s/N_0 = 17.5$ dB. The solid lines represent the theoretical values [7] and the markers are the measured values. Again, the measurements come very close to theoretical. For reference, the theoretical performance curve for no system noise is also shown. It follows $P_b=\rho/2$ for $\rho \leq 8/SJR$ and is zero for $\rho>8/SJR$. The break points are shown as vertical dashed lines. The predicted improvement in worst case operation when system noise was added

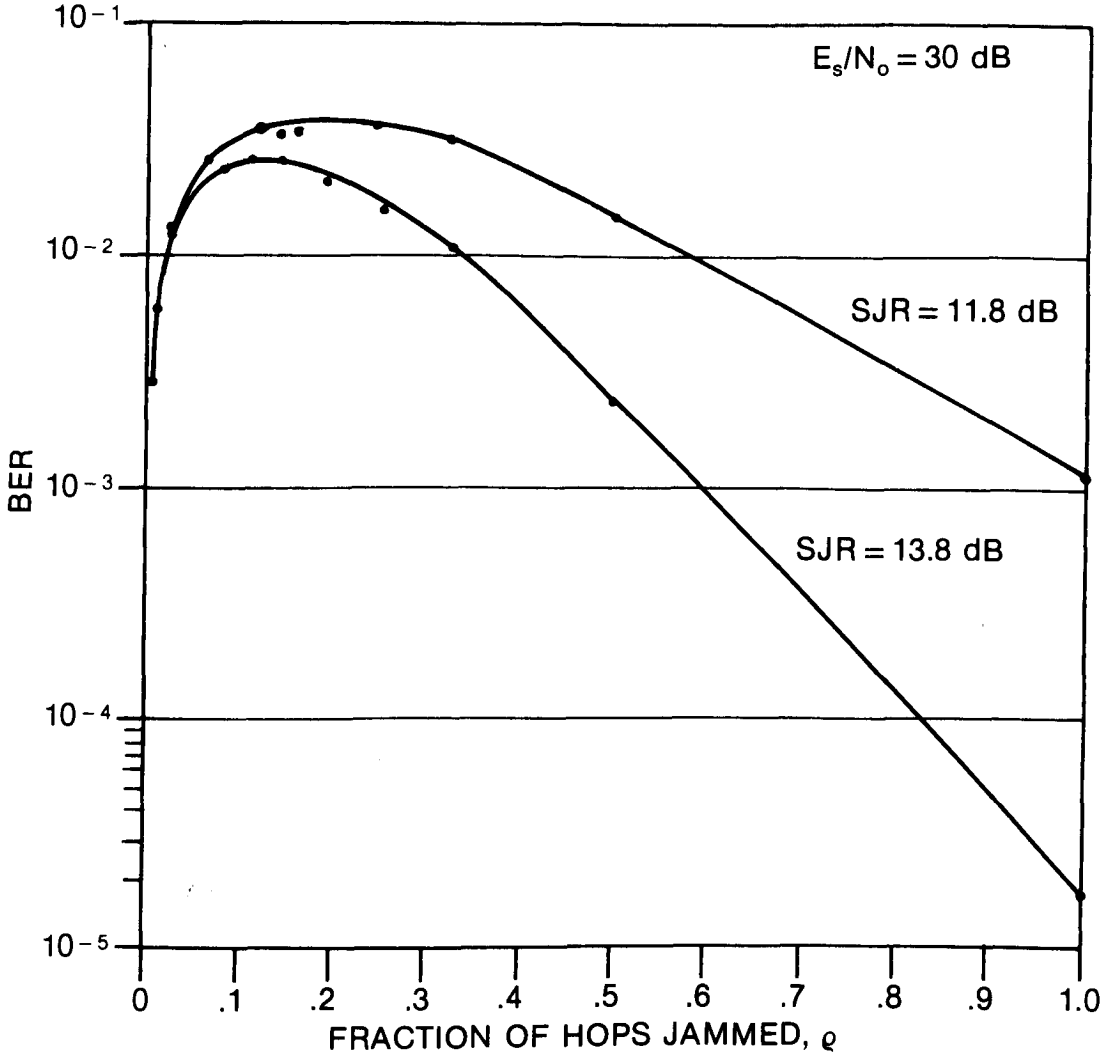

Fig. 3.17. The bit error rate measured for 8-ary FSK in the presence of PBN jamming as a function of ρ for E_s/N_0 = 30 dB and 2 values of E_s/J_0.

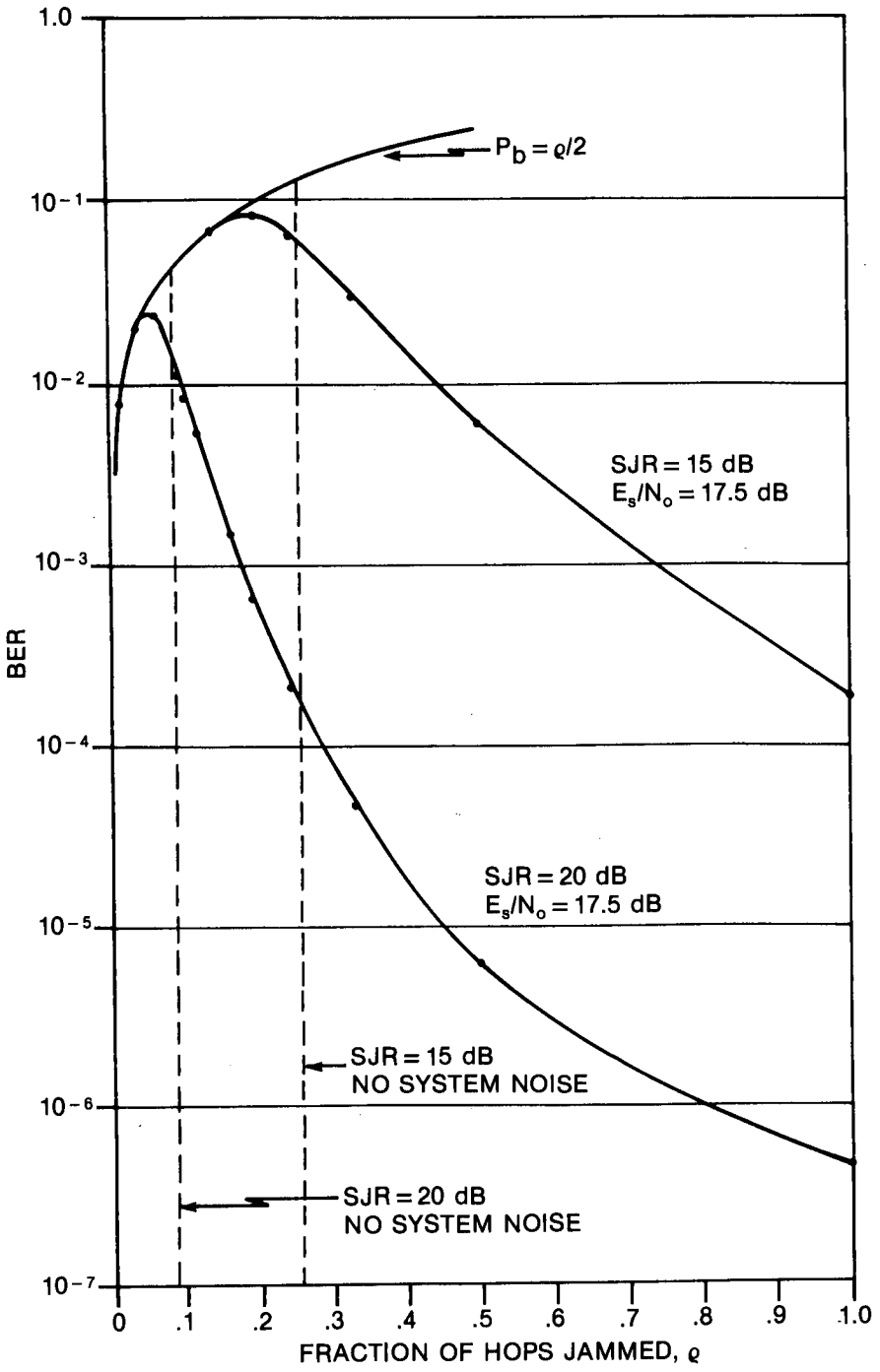

Fig. 3.18. The bit error rate measured for 8-ary FSK in the presence of MT jamming for E_s/N_0 = 17.5 dB and 2 values of E_s/J_0.

was observed. The sharp peak in worst case performance shows the degradation a tone jammer can inflict even when a large SJR, such as 20 dB in Fig. 3.18, is available.

4. CONCLUSION

A SAW-based demodulator for M-ary NCFSK has been built and demonstrated. Measurements showed that its implementation loss was a very respectable 0.5 dB. The flexibility of the measurement system and the capability of changeable window functions led to the confirmation of previously developed theories and conjectures. In particular, the measurements confirmed the analysis developed in [7] describing the performance in the presence of MT and PBN jamming plus system noise. As expected, full windowing improved performance in the presence of severe (20% of tone spacing) frequency errors and provided 26 dB protection against worst case interchannel interference (i.e. a signal in an adjacent channel must be +26 dB above the signal before any noticeable errors are caused). However, in other performance measurements such as in the presence of tone jammers, and with smaller frequency errors ($\leq$10%), the rectangular window proved as good or better than the full window. It was discovered that the so called "intermediate" window function had a number of performance characteristics indicating its desirability compared to both the rectangular and the KB window.

Although implemented in an experimental measurement system, the SAW analyser was seen to be an excellent candidate as an actual onboard processor provided a few of its characteristics are upgraded. Its best sidelobe level of -30 dB would have to be improved if the power of the signal in adjacent channels differed by more than 26 dB. The 50-dB dynamic range set by internal analyser noise and SAW device spurious signals was sufficient for the measurement system. However, in a practical system with large differences between adjacent users, it may be desirable to have a larger dynamic range. The limited linear response range shown in Fig. 3.1 did not affect the measurement system. However, if deemed a problem in a future system the linear range could likely be extended by improved envelope detector and amplifier circuitry.

Since the SAW analyzer shows such good potential as an onboard-the-satellite demodulator, not only from a technical but from a cost point of view, work has already begun at Com Dev Limited in Cambridge, Ontario on an advanced developmental model. This system will have major improvements over the SAW analyzer used in the measurement system described here. It will be capable of the desired integration or transform time of 50 μs and also will be capable of 100% duty cycle. The reflective array compressor transducer structure will replace the older interdigital finger transducer structure [2]. Windowing will be built into the SAW devices and will give sidelobe levels >40 dB down from the main peak for improved performance against interchannel interference. The dynamic range due to internal noise should exceed the 50 dB achieved with the present analyzer. Finally, some attention is being paid to keeping weight, volume, and power consumption to within limits supportable on a spacecraft and to making devices that can function properly in the space environment.

In summary, a very powerful measurement system was developed that led not only to confirmation of previous theories and conjectures but provided new insights and discoveries. More importantly, it provided considerable confidence in proceeding with a much larger scale effort, the advanced developmental model.

5. ACKNOWLEDGEMENT

The author's would like to acknowledge Dr. J.S. Bird of CRC who performed the theoretical calculations for the PBN and MT jamming performance. It is noted that there was no known exact analytical technique for MT performance in the presence of system noise until Dr. Bird devised the one used for the analysis in this report.

6. REFERENCES

[1] M.A. Jack, P.M. Grant, and J.H. Collins, "The theory, design, and application of surface acoustic wave Fourier-transform processors," Proc. IEEE, vol. 68, pp. 450-468, April 1980.

[2] P.F. McKenzie, D.B. Coomber, and B.H. Hutchinson Jr., "Design and performance of a SAW-based MFSK demodulator," IEEE Nat. Telecom. Conf. Record, pp. 22.6.1-22.6.5, 1980, IEEE Cat. No. CH1539-6/80.

[3] F.J. Harris, "On the use of windows for harmonic analysis with the discrete Fourier transform," Proc. IEEE, Vol. 66, pp. 51-83, January 1978.

[4] J.M. Wozencraft and I.M. Jacobs, Principles of Communication Engineering, New York: Wiley, 1965, p. 577.

[5] L.S. Metzger, D.M. Boroson, and J.J. Urhan, "Receiver windowing for FDM MFSK signals," IEEE Trans. Comm., vol. COM-27, pp. 1519-1526, October 1979.

[6] P.H. Wittke, P.J. McLane, and P. Ma, "Study of the reception of frequency dehopped M-ary FSK," Research Report No. 83-1, Dept. of Elect. Eng., Queen's Univ., Kingston, Ontario, March 1983.

[7] J.S. Bird and E.B. Felstead, "Anti-jam performance of fast frequency-hopped M-ary NCFSK - An Overview," Accepted for publication in IEEE Trans. Comm., October 1985.

APPENDIX: SOME CIRCUIT DETAILS

The simplified description of the demodulator implementation was given in the main text. The general block diagram is given in Fig. 2.3 and a simplified timing diagram is given in Fig. 2.7. In this appendix, some further details are given but still in rather broad outline. No steps were taken to optimize the circuitry. Therefore the circuits shown are ones that work but further optimization may be possible.

In Fig. A.1 a simplified block diagram is shown for the section that makes a decision as to which tone was received. The analog-to-digital converter is a TRW model TDC1025E/C, 8-bit flash converter. It was clocked at 1.6 MHz which provided the samples at 625 ns intervals required to sample each M-ary frequency slot. Register Y is initially loaded with a threshold level at the same time that register X is initially loaded with the first frequency slot data sample. If register X was greater than register Y then the second data sample would be loaded into register Y. However, if register X had been less than register Y, then the second sample would have been loaded into register X. This process is continued for the 4, 8, or 16 slots as set by the user reset counter (B_1 and B_2 on the second timing generator card). The slot count of the largest sample in a user channel is stored in register D1 and transferred to user A (F1) or user B (H1) register at the end of M samples for 1 user. This process is repeated for each user channel using a common threshold setting.

In Fig. A.2 is illustrated the fact that the interface to the Rockland frequency synthesizer is simply implemented by storing the synthesizer input data in a PROM at the appropriate address. A limiting amplifier is needed on the output of the synthesizer in order to maintain equal amplitude of the tones. Figs. A.3 through A.8 inclusive are given without comment. They provide some of the circuit details on items previously mentioned in outline only.

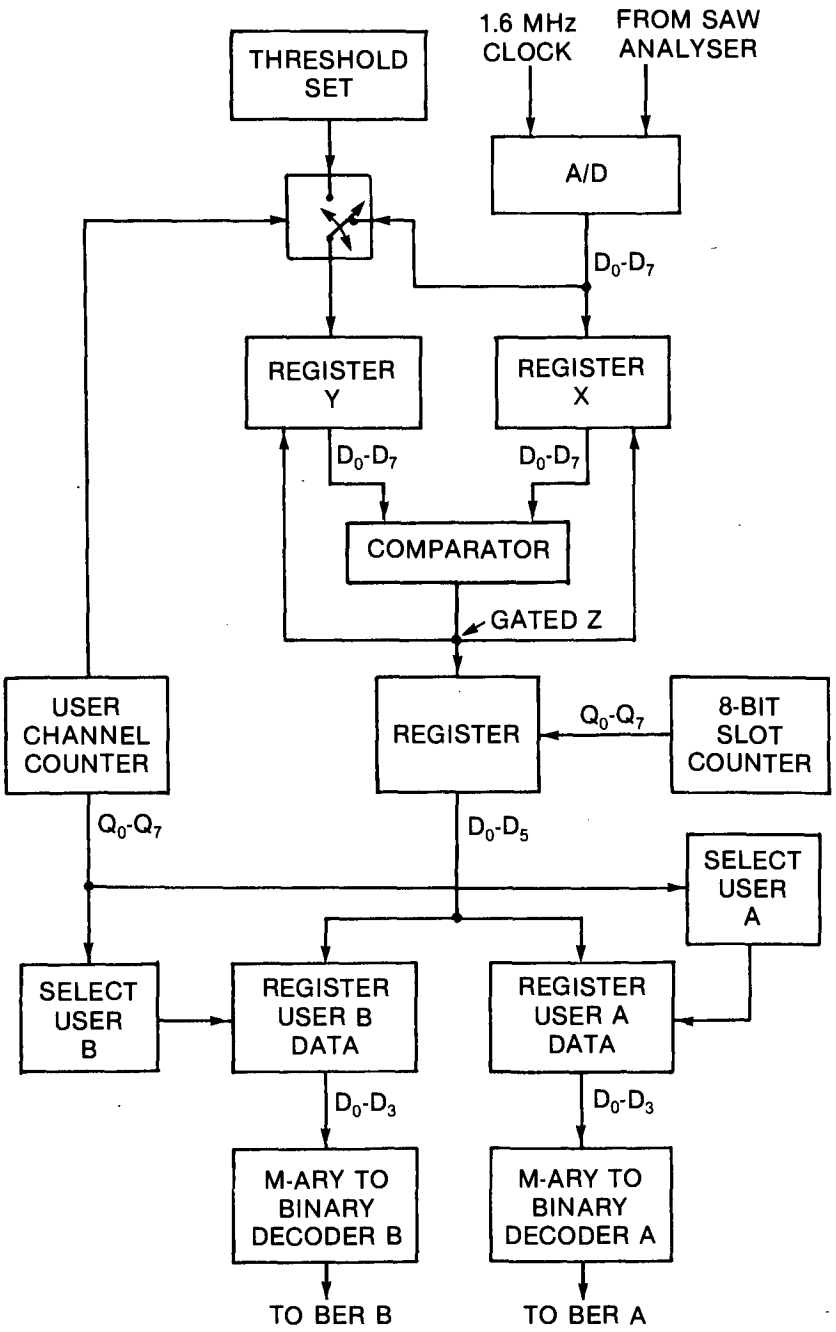

Fig. A.1. A simplified block diagram for the decision and decoding sections. Timing and clock lines are not shown.

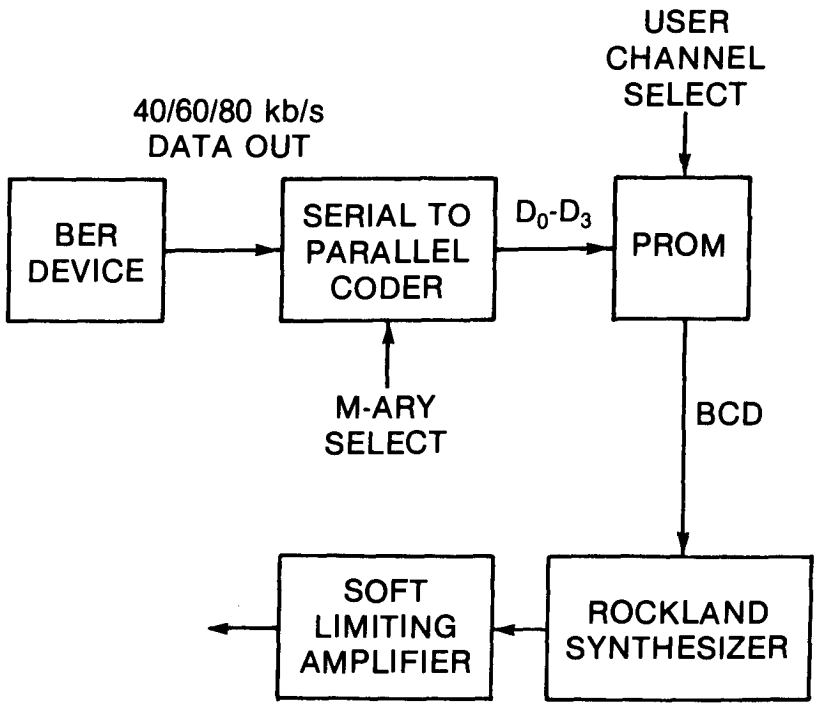

Fig. A.2. A simplified block diagram for the M-ary tone generating section. It is repeated for second and subsequent users.

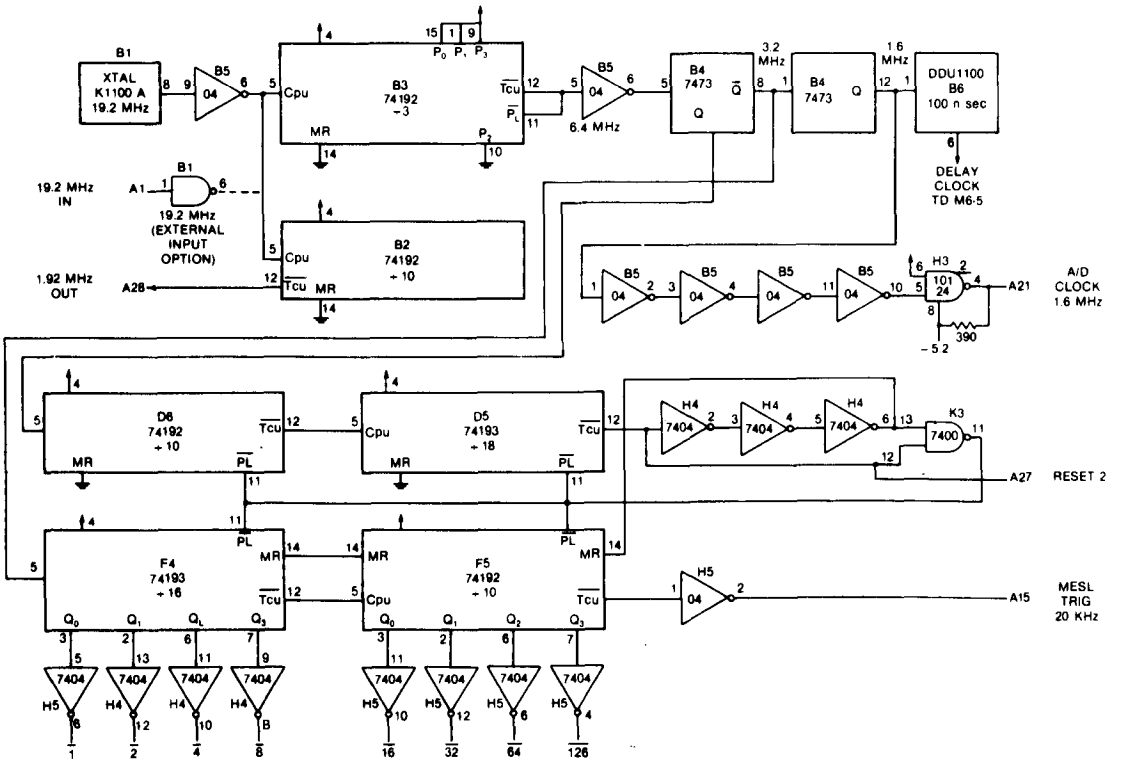

Fig. A.3. The timing generator/comparator card.

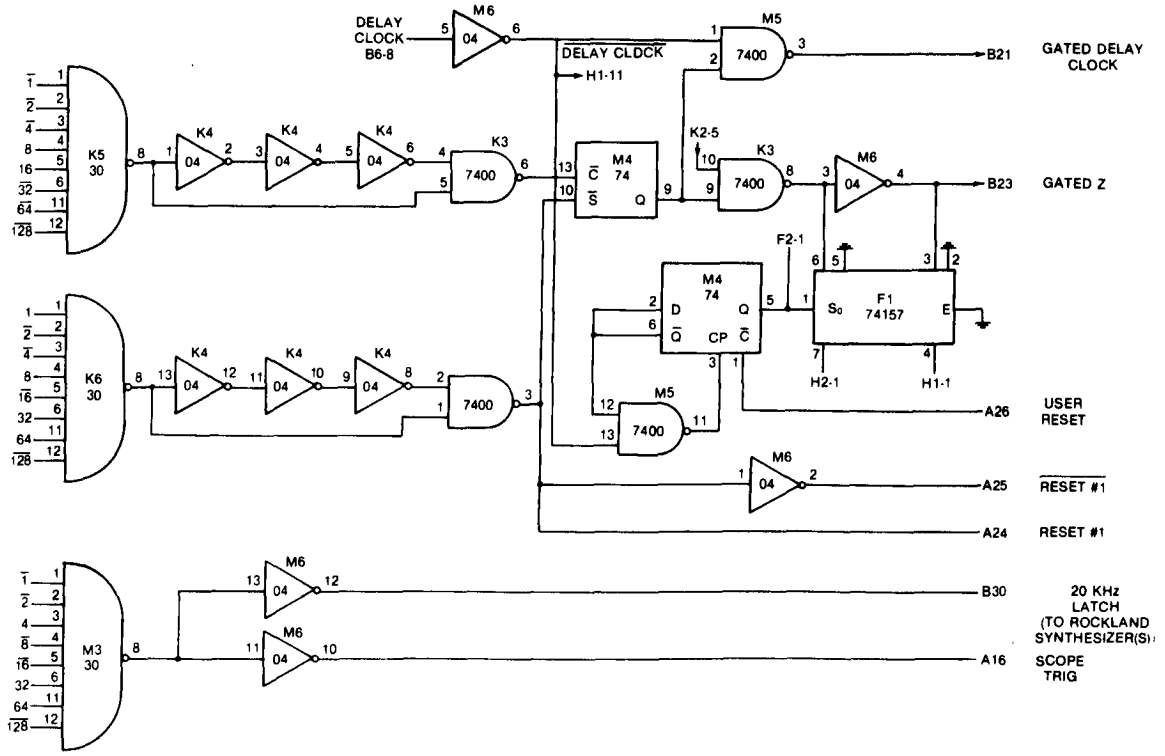

Fig. A.4. The timing generator/comparator card, continued.

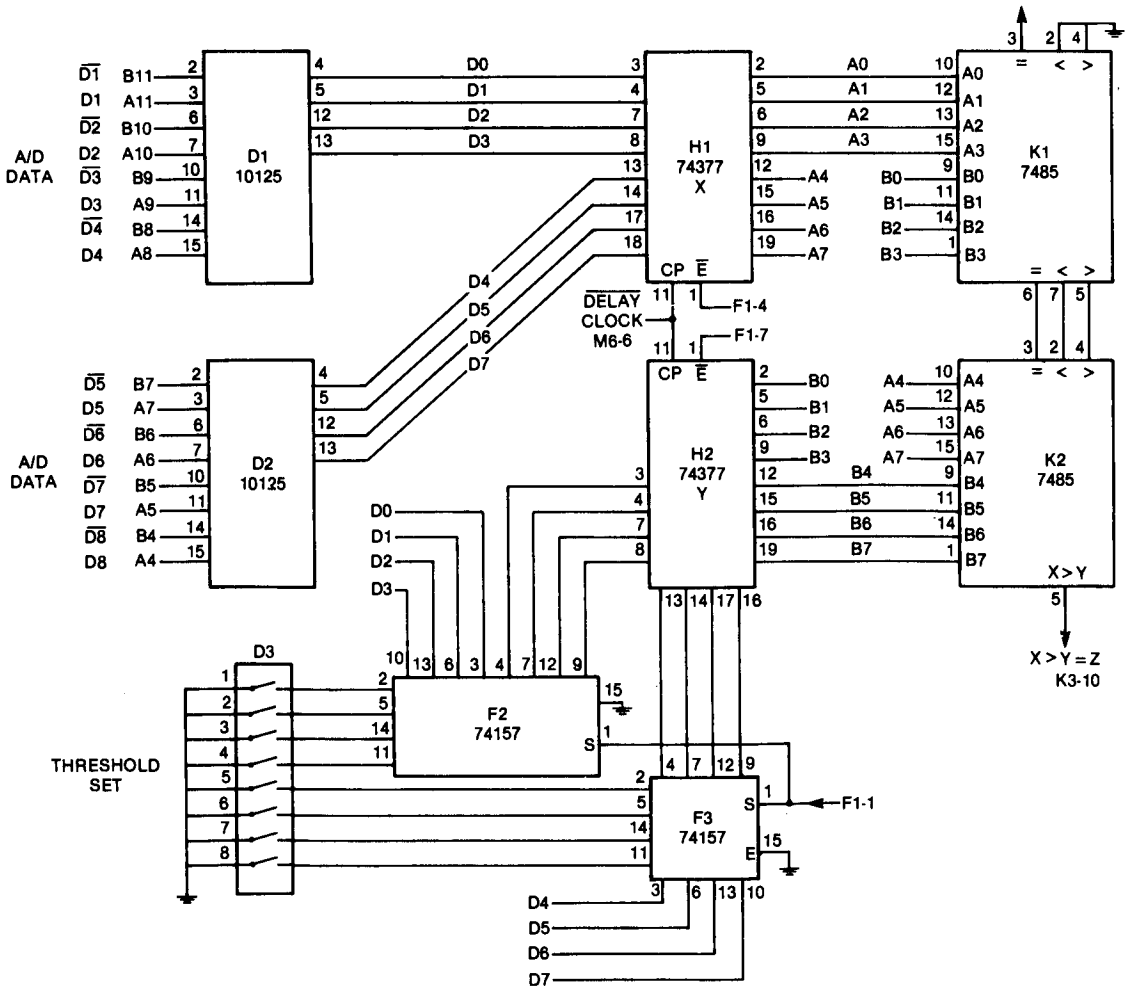

Fig. A.5. The timing generator/comparator card, continued.

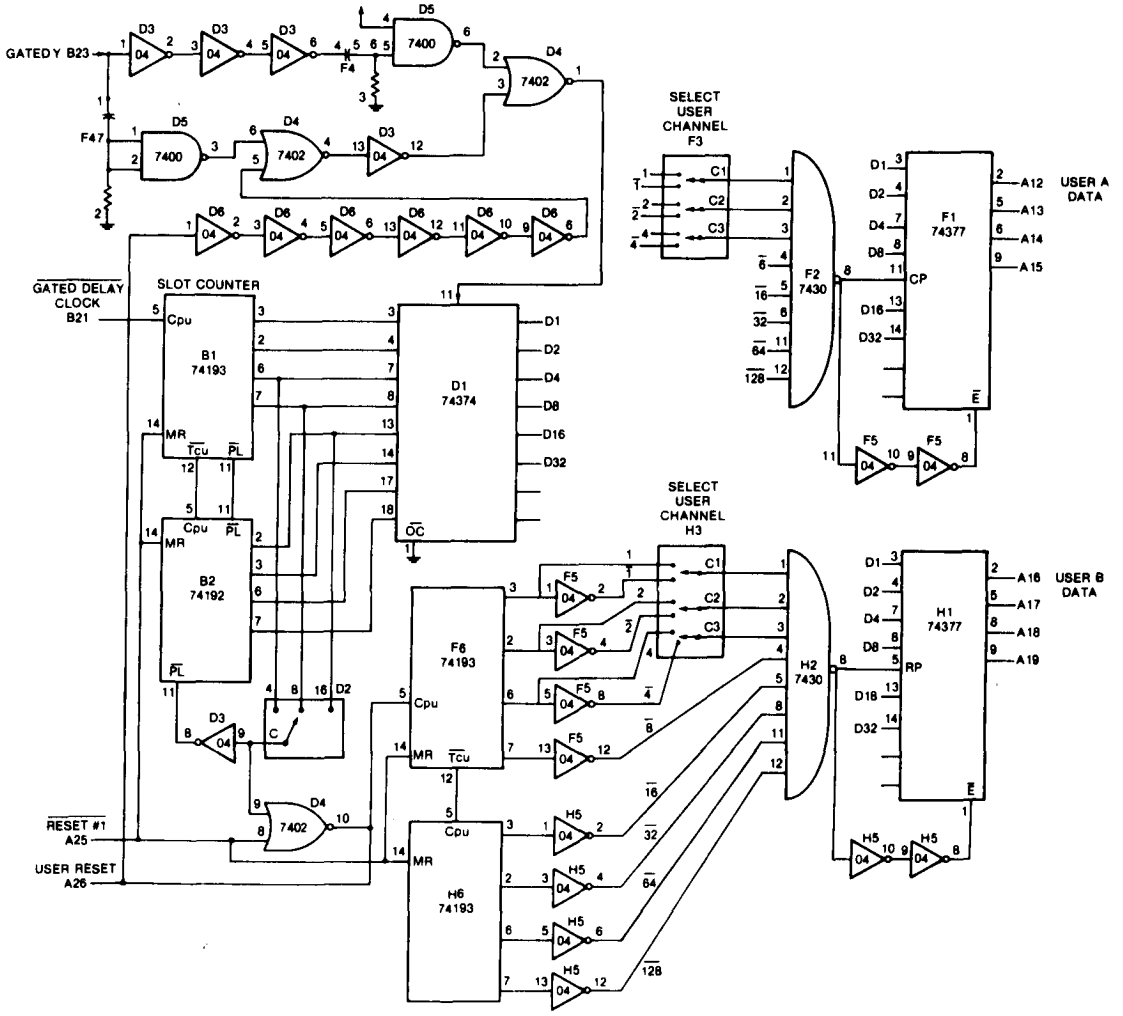

Fig. A.6. The second timing generator card.

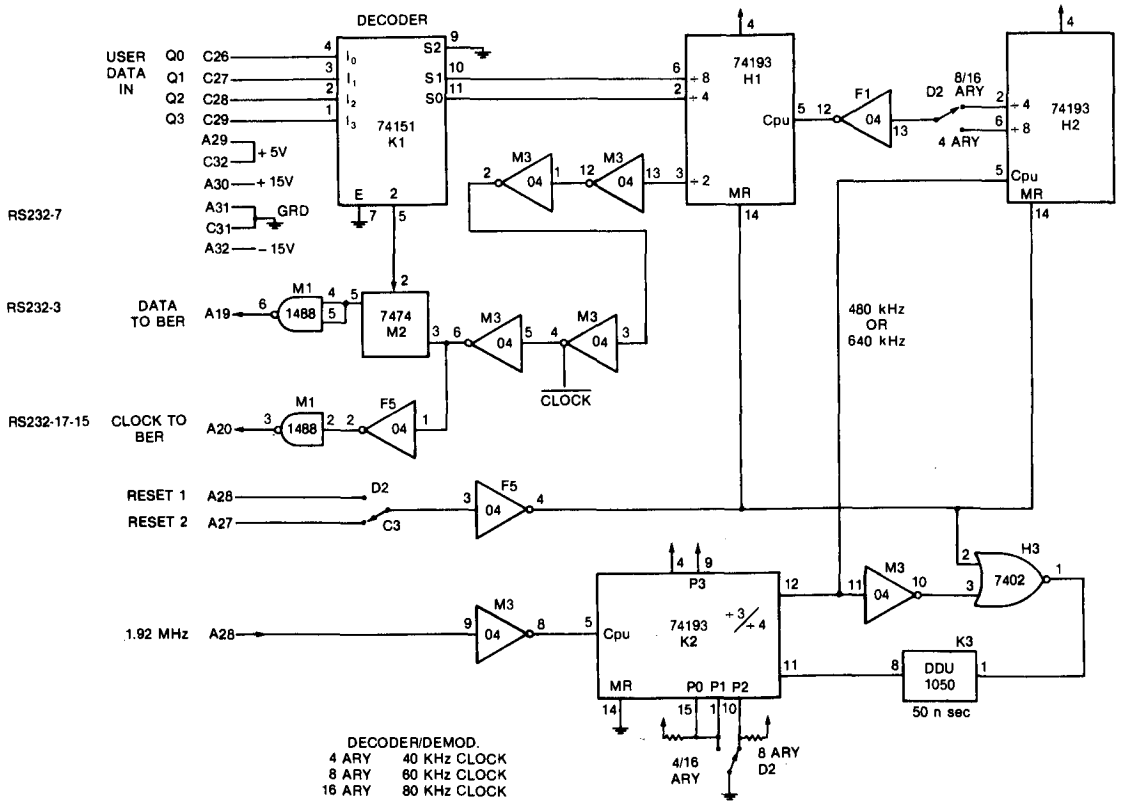

Fig. A.7. The user card A or B showing decoder.

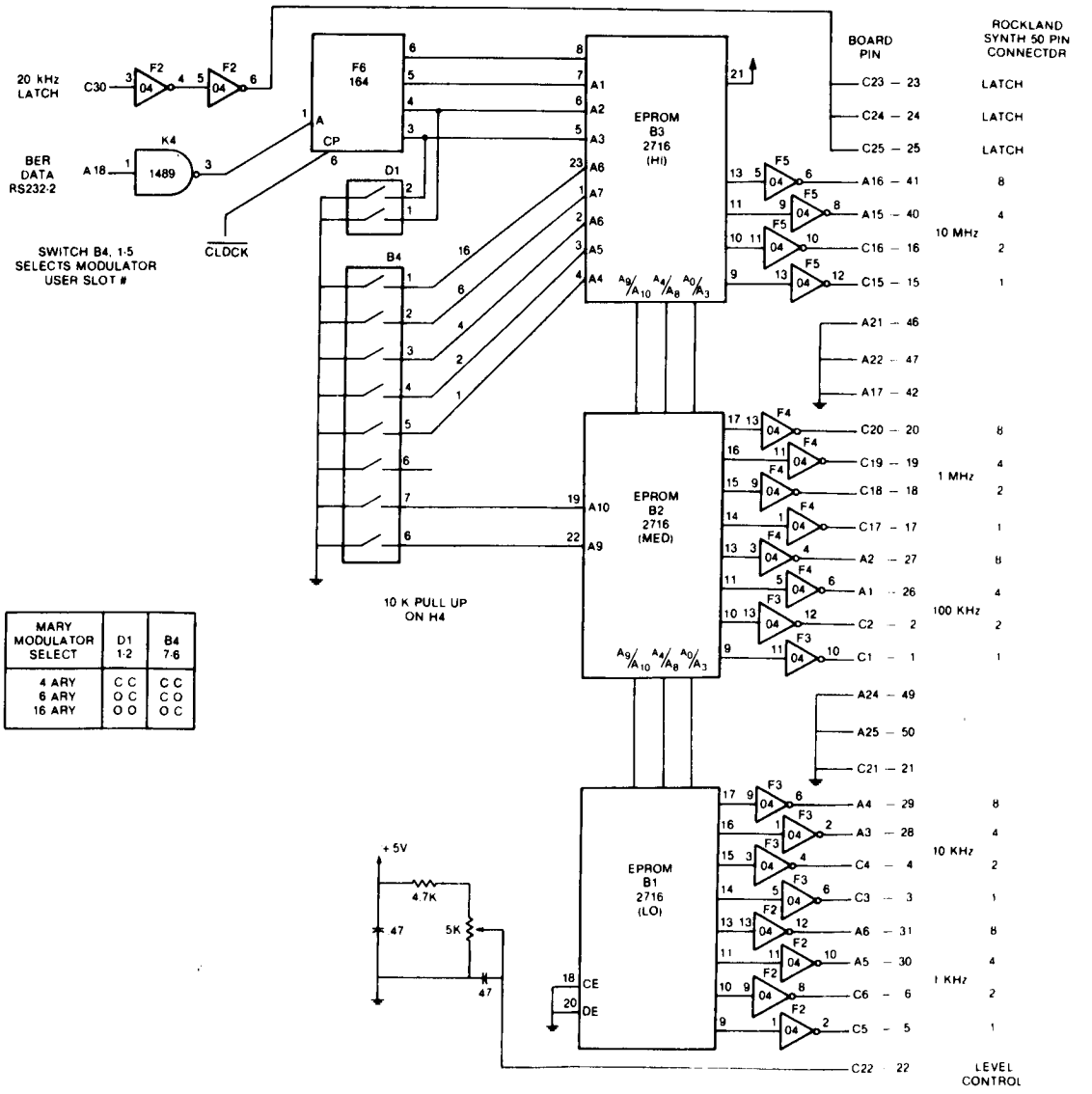

MARY MODULATOR SELECT	D1 1-2	B4 7-6
4 ARY	C C	C C
6 ARY	O C	C O
16 ARY	O O	O C

Fig. A.8. The user card A or B showing the BER to synthesizer interface.

Unclassified

Security Classification

DOCUMENT CONTROL DATA - R & D

(Security classification of title, body of abstract and indexing annotation must be entered when the overall document is classified)

1. ORIGINATING ACTIVITY
Communications Research Centre
Box 11490, Station 'H', Ottawa, K2H 8S2

2a. DOCUMENT SECURITY CLASSIFICATION
Unclassified

2b. GROUP

3. DOCUMENT TITLE
A SAW-based demodulator for multiple-user dehopped M-ary FSK signals - implementation and measurements

4. DESCRIPTIVE NOTES (Type of report and inclusive dates)
Technical Report

5. AUTHOR(S) (Last name, first name, middle initial)
Felstead, E.B., Pearce, J.L., and Selin, D.L.

6. DOCUMENT DATE
June 1985

7a. TOTAL NO. OF PAGES
43

7b. NO. OF REFS
7

8a. PROJECT OR GRANT NO.
CRAD Project No. 32A58

9a. ORIGINATOR'S DOCUMENT NUMBER(S)
CRC Technical Report No. 1392

8b. CONTRACT NO.

9b. OTHER DOCUMENT NO.(S) (Any other numbers that may be assigned this document)

10. DISTRIBUTION STATEMENT
UNLIMITED

11. SUPPLEMENTARY NOTES

12. SPONSORING ACTIVITY
DCEM for CRAD at CRC under the Defence R&D Program in DOC

13. ABSTRACT

A demodulator has been built and tested that is capable of performing the functions of an onboard-the-satellite processor for receiving M-ary noncoherent FSK signals with multiple users being separated by FDMA. It is based on spectral analysis of the received signal by an analog chirp transformer implemented with surface acoustic-wave devices. Demodulation of M=4-, 8-, and 16-ary FSK signals of 25-μs symbol duration was demonstrated with capability of handling up to 40/M users. An implementation loss was only 0.5 dB. Measurement of bit error rate performance in the presence of system noise, frequency errors, and partial-band-noise and multiple-tone jamming were made and found to agree well with theory. The effects were examined of three different time windows: rectangular, Kaiser Bessel $\alpha = 1.6$, and one intermediate between these two. The intermediate window is promising because of low window loss combined with good adjacent channel interference tolerance.

Unclassified

Security Classification

KEY WORDS

Demodulator, M-ary FSK, multiple access, satellite communications, frequency hopping, surface acoustic wave, chirp transform, partial band jamming, tone jamming, windows

INSTRUCTIONS

1. ORIGINATING ACTIVITY: Enter the name and address of the organization issuing the document.

2a. DOCUMENT SECURITY CLASSIFICATION: Enter the overall security classification of the document including special warning terms whenever applicable.

2b. GROUP: Enter security reclassification group number. The three groups are defined in Appendix 'M' of the DRB Security Regulations.

3. DOCUMENT TITLE: Enter the complete document title in all capital letters. Titles in all cases should be unclassified. If a sufficiently descriptive title cannot be selected without classification, show title classification with the usual one-capital-letter abbreviation in parentheses immediately following the title.

4. DESCRIPTIVE NOTES: Enter the category of document, e.g. technical report, technical note or technical letter. If appropriate, enter the type of document, e.g. interim, progress, summary, annual or final. Give the inclusive dates when a specific reporting period is covered.

5. AUTHOR(S): Enter the name(s) of author(s) as shown on or in the document. Enter last name, first name, middle initial. If military, show rank. The name of the principal author is an absolute minimum requirement.

6. DOCUMENT DATE: Enter the date (month, year) of Establishment approval for publication of the document.

7a. TOTAL NUMBER OF PAGES: The total page count should follow normal pagination procedures, i.e., enter the number of pages containing information.

7b. NUMBER OF REFERENCES: Enter the total number of references cited in the document.

8a. PROJECT OR GRANT NUMBER: If appropriate, enter the applicable research and development project or grant number under which the document was written.

8b. CONTRACT NUMBER: If appropriate, enter the applicable number under which the document was written.

9a. ORIGINATOR'S DOCUMENT NUMBER(S): Enter the official document number by which the document will be identified and controlled by the originating activity. This number must be unique to this document.

9b. OTHER DOCUMENT NUMBER(S): If the document has been assigned any other document numbers (either by the originator or by the sponsor), also enter this number(s).

10. DISTRIBUTION STATEMENT: Enter any limitations on further dissemination of the document, other than those imposed by security classification, using standard statements such as:

(1) "Qualified requesters may obtain copies of this document from their defence documentation center."

(2) "Announcement and dissemination of this document is not authorized without prior approval from originating activity."

11. SUPPLEMENTARY NOTES: Use for additional explanatory notes.

12. SPONSORING ACTIVITY: Enter the name of the departmental project office or laboratory sponsoring the research and development. Include address.

13. ABSTRACT: Enter an abstract giving a brief and factual summary of the document, even though it may also appear elsewhere in the body of the document itself. It is highly desirable that the abstract of classified documents be unclassified. Each paragraph of the abstract shall end with an indication of the security classification of the information in the paragraph (unless the document itself is unclassified) represented as (TS), (S), (C), (R), or (U).

The length of the abstract should be limited to 20 single-spaced standard typewritten lines; 7½ inches long.

14. KEY WORDS: Key words are technically meaningful terms or short phrases that characterize a document and could be helpful in cataloging the document. Key words should be selected so that no security classification is required. Identifiers, such as equipment model designation, trade name, military project code name, geographic location, may be used as key words but will be followed by an indication of technical context.